Geological Society, London, Special Publications Online First

Calculating anisotropic piezoelectric properties from texture data using the MTEX open source package

David Mainprice, Florian Bachmann, Ralf Hielscher, Helmut Schaeben and Geoffrey E. Lloyd

Geological Society, London, Special Publications, first published July 22, 2014; doi 10.1144/SP409.2

Notes

Calculating anisotropic piezoelectric properties from texture data using the MTEX open source package

DAVID MAINPRICE[1]*, FLORIAN BACHMANN[2], RALF HIELSCHER[3], HELMUT SCHAEBEN[2] & GEOFFREY E. LLOYD[4]

[1]*Geosciences Montpellier UMR CNRS 5243, Université Montpellier 2, 34095 Montpellier Cedex 05, France*

[2]*Mathematische Geologie und Geoinformatik, Institut für Geophysik und Geoinformatik, Technische Universität Freiberg, 09596 Freiberg, Germany*

[3]*Fakultät für Mathematik, Technische Universität Chemnitz, 09126 Chemnitz, Germany*

[4]*School of Earth and Environment, The University, Leeds LS2 9JT, UK*

**Corresponding author (e-mail: David.Mainprice@gm.univ-montp2.fr)*

Abstract: This paper presents the background for the calculation of anisotropic piezoelectric properties of single crystals and the graphical display of the results in two or three dimensions, and the calculation of the aggregate properties from constituent crystals and the texture of the aggregate in a coherent manner. The texture data can be obtained from a wide range of sources, including pole figure diffraction and single orientation measurements (electron backscattered diffraction, electron channelling pattern, Laue Pattern, optical microscope universal-stage). We consider the elastic wave propagation in piezoelectric crystals as an example of the interaction of electrical (2nd rank tensor), piezoelectric (3rd rank tensor) and elastic properties (4th rank tensor). In particular, we give explicit formulae for the calculation of the Voigt averaged tensor from individual orientations or from an orientation distribution function. For the latter we consider numerical integration and an approach based on the expansion into spherical harmonics. We illustrate the methods using single crystals, polycrystalline quartz measured using electron channelling patterns and ideal Curie limiting groups applied to quartz aggregates. This paper also serves as a reference paper for the mathematical tensor capabilities of the texture analysis software MTEX.

The word piezoelectricity is derived from the Greek word for 'to press' (*piezein*), hence pressure causing electricity or piezoelectricity. Piezoelectric properties are of a wide interest in science as the effect has now been reported in inorganic single crystals (e.g. α-quartz; Bechmann 1958), organic crystals (e.g. sodium oxalate; Haussühl 1991), molecular crystals (e.g. 2-furyl methacrylic anhydride; Kerkoc *et al.* 1999), inorganic polycrystals (e.g. ceramics; Messing *et al.* 2004), polymers (e.g. Hayakawa & Wada 1973), bone (e.g. Fukada & Yasuda 1957), collagen (e.g. Fukada & Yasuda 1964) and wood (e.g. Bazhenov 1961). Industrial interest in piezoelectricity for transducers and resonators stems from the nature of the effect, which is either the direct effect (when stress is applied to the material and a polarized electric field develops) or the converse effect (when an electric field is applied to the material it becomes strained). On 8 April 1880, Jacques Curie reported to the French Society of Mineralogy his discovery (with the collaboration of his brother Pierre) of the direct piezoelectric effect in five crystal species examined: tourmaline (point group shown in **bold**, **3 m**); sphalerite (ZnS, $\bar{\mathbf{4}}$**3 m**); boracite ($Mg_3B_7O^{13}Cl$, **mm 2**); zincite (ZnO, **6 mm**); and α-quartz (SiO_2, **32**) (Curie & Curie 1880). Here we have used modern mineral names. The existence of the converse effect was predicted from thermodynamic arguments by Lippmann (1881). However, by the end of 1881 the Curie brothers had experimentally observed the converse effect and confirmed that both effects are due to the same physical property (Curie & Curie 1881, 1882). In 1893 Jacques Curie became head lecturer in mineralogy at the University of Montpellier, where his last work was to determine the piezoelectric constants of α-quartz in 1910 before retiring due to poor health (Cady 1964). The formal description of piezoelectricity in tensor notation for all crystallographic classes is due to Woldemar Voigt's major contribution summarized in his two books *Die Fundamentalen Physiklischen Eigenschaften der Kristalle* (1898) and the better-known *Lehrbuch der Kristallphysik* (1910, 1928).

Industrial application of piezoelectric single crystals was probably first envisaged by Paul Langevin who invented an ultrasonic generator using quartz and steel plates, a precursor of modern

From: Faulkner, D. R., Mariani, E. & Mecklenburgh, J. (eds) *Rock Deformation from Field, Experiments and Theory: A Volume in Honour of Ernie Rutter*. Geological Society, London, Special Publications, **409**, http://dx.doi.org/10.1144/SP409.2

sonar device, around 1917. Subsequently the use of piezoelectric single crystals (mainly quartz) in resonators, filters and transducers became widespread. Single-crystal quartz is still widely used today along with crystals of new compositions, such as langasite, with improved characteristics (Jung & Auh 1999). Piezoelectric polycrystalline ceramics (Jaffe *et al.* 1971), often composed of two ferroelectric phases, are now more widely used than single crystals in transducers. In this paper we will use terms crystal-preferred orientations (CPOs), or textures as they are referred to in Materials Science, interchangeably as no possible confusion can result in present context. Enhancing of the CPOs of ceramics is motivated by the need to increase the piezoelectric strain for a given applied voltage in transducer applications. Many single crystals exhibit strongly anisotropic piezoelectric properties and many aggregates of piezoelectric crystals also have strong CPOs. In polycrystalline aggregates, the CPO may be due to the plastic deformation in geological samples or specially devised mechanical processing in industrial applications. In industrial processing, the application of strong electric fields can be used to enhance the degree of alignment of ferro-electric dipoles in ferroelectric crystals (e.g. perovskite structured double oxides $BaTiO_3$, $KNbO_3$, $KTaO_3$ and $PbTiO_3$ and double fluorides $KMgF_3$ and $KZnF_3$), a technique known as poling (Messing *et al.* 2004). CPO is often partially described by pole figures in ceramics, whereas the CPO can be described completely and concisely in a quantitative manner by the orientation density function (ODF). The combination of strong CPOs and anisotropic single-crystal properties results in a strong directional variation in specimen properties, which are often difficult and time-consuming to completely characterize by laboratory measurements in many directions. The evaluation of several physical properties of interest in piezoelectric materials from CPO – such as the the 2nd rank dielectric permittivity, 3rd rank piezoelectric strain and 4th rank elastic stiffness tensors needed for elastic wave propagation – allows the determination of aggregate properties over the complete orientation sphere of the specimen reference frame.

The estimation of physical properties of crystalline aggregates from the properties of the component crystals has been the subject of extensive literature since the classical work of Voigt (1887) and Reuss (1929). Such a simple volume averaging approach is only feasible if the bulk properties of the crystals dominate the physical property of the aggregate and the effects of grain boundary interfaces can be ignored, such as the electrical conductivity along grain boundaries. In the case of piezoelectic properties, the Reuss bound cannot be implemented as the piezoelectric 3rd rank tensors are only transposable and not invertible (unlike 2nd and 4th rank centrosymmetric tensors, which are both transposable e.g. 2nd rank tensor T to T^{T} and invertible e.g. T to T^{-1}). A further complication in piezoelectric materials is the coupled interaction between several thermal, electrical and mechanical variables, which requires a more rigorous thermodynamic definition of the measurement of the tensor property and constitutive equations for their application to given problems as illustrated later. In this paper we will be restricted to the simple Voigt volume-averaging approach for aggregates and to the propagation of elastic waves in a piezoelectric material as an example of electromechanical coupling. Other averaging methods, such as self-consistent and variational effective medium methods, are beyond the scope of the present paper.

A piezoelectric effect has been established either quantitatively or qualitatively in only 30% of 239 minerals that do not have a centre of symmetry and hence should be piezoelectric (Parkhomenko 1971). The semi-conducting elements tellurium (Te) and selenium (Se), along with the mineral pyrolusite (MnO_2), have the greatest piezoelectric effect of naturally occurring compounds. Minerals with strong effect include greenockite (CdS), cadmosetite (β-CdSe) and zincite (ZnO), which have an effect 3–5 times greater than α-quartz. However, there are over 70 minerals that have a piezoelectric effect of similar magnitude to α-quartz. Piezoelectric minerals occur most frequently in ore deposits (52 references), followed by veins and hydrothermal associations (24 references) and volcanic rocks (18 references) as documented by Parkhomenko (1971). Ore deposits are often associated with hydrothermal activity in volcanic rocks, so these categories are not mutually exclusive. As can be seen in an area as critical to the Earth's non-renewable resources as ore deposits, piezoelectric minerals may have an important role for exploration. The interest of the electronic industry in piezoelectric minerals does not require development here. As show by Parkhomenko (1971), the accurate determination of the piezoelectric tensors of minerals has only been made for a very small fraction of piezoelectric minerals.

Although piezoelectric minerals are generally not very common in the Earth's crust, one *is* very common: quartz is the third-most common mineral at about 12% of the Earth's crust, according to Taylor & McLennan (1985). The presence of significant volumes of quartz will influence the seismic properties of common crustal rock types such as sandstone, quartzite and granite. Some piezoelectric minerals are locally highly concentrated such as sulphide and oxide minerals in ore deposits, which are the subject of intensive geophysical exploration in Russia (and more recently in western countries;

Bishop & Emerson 1999; Neishtadt *et al.* 2006). To our knowledge the implications of the piezoelectric effect for wave propagation of minerals has never been evaluated.

This paper is designed as a reference for Earth and material scientists who want to use the texture analysis software MTEX (Hielscher & Schaeben 2008) to compute piezoelectric tensor properties of single crystals and aggregates from constituent crystal properties and the texture of the aggregate. MTEX is a comprehensive, freely available MatLab toolbox that can be applied to a wide range of problems in quantitative texture analysis such as ODF modelling, pole figure to ODF inversion, EBSD data analysis, and grain modelling. The MTEX toolbox can be downloaded from http://mtex.googlecode.com. Unlike many other texture analysis programs, it offers a programming interface which allows for the efficient processing of complex research problems in the form of scripts (M-files). The MatLab® environment provides a wide variety of high-quality graphics file format to aid publication and display of the results. In addition the MTEX toolbox will work identically on Microsoft Windows, Apple Mac OSX and Linux platforms in 32- and 64-bit modes with a simple installation procedure.

In MTEX, texture analysis information such as ODFs, EBSD data and pole figures are represented by variables of different types. For example, in order to define a unimodal ODF with half-width 10°, modal-preferred orientation (10°, 20°, 30°) Euler angles and trigonal crystal symmetry of quartz, one issues the command

```
myODF = unimodalODF(orientation
        ('Euler', 10*degree,
        20*degree,30*degree),...
        symmetry('-3m'),
        'halfwidth', 10*degree)
```

which generates a variable myodf of type ODF which is displayed as

```
myODF = ODF (show methods, plot)
  crystal symmetry : -3m, X||a*,
                     Y||b, Z||c*
  sample symmetry  : triclinic

  Radially symmetric portion:
    Kernel : de la Vallee Poussin, hw = 10
    Center : (10, 20, 30)
    Weight : 1
```

We will keep this style of displaying input and output to make the syntax of MTEX as clear as possible. Note that there is also an exhaustive interactive documentation included in MTEX, which explains the syntax of each command in detail. This paper is the sequel to our previous paper (Mainprice *et al.* 2011) on the 2nd and 4th rank symmetric tensors of crystal and polycrystal anisotropic physical properties. To conform with the symbols used in our previous paper, we will use the notation ε for strain, σ for stress and S for entropy; in many texts on piezoelelectricty (e.g. Mason 1966; Ikeda 1990; Royer & Dieulesaint 1996; Tichý *et al.* 2010) the symbols S for strain, T for stress and σ for entropy are used. To avoid any potential confusion all the symbols and SI units used in this paper for tensors are listed in Table 1.

Fundamentals of piezoelectric tensors

In what follows we give the necessary background to undertake piezoelectric property calculations for single crystals, without the full mathematical developments that can be found elsewhere (e.g. Cady 1964; Mason 1966; Nye 1985; Ikeda 1990; Newnham 2005; Tichý *et al.* 2010). We restrict

Table 1. *Symbols and units used for tensors this paper*

Tensor	Rank	Symbol	SI Units
Elastic strain	2nd	ε_{ij}	Dimensionless
Elastic stress	2nd	σ_{ij}	Pa
Electric field	1st	E_i	$V\,m^{-1}$
Electric displacement	1st	D_i	$C\,m^{-2}$
Dielectric permittivity	2nd	κ_{ij}	$F\,m^{-1}$
Dielectric impermeability	2nd	β_{ij}	$m\,F^{-1}$
Dielectric polarization	1st	P_i	$C\,m^{-2}$
Elastic stiffness	4th	c_{ijkl}	Pa
Elastic compliance	4th	s_{ijkl}	Pa^{-1}
Piezoelectric strain	3rd	d_{ijk}	$C\,N^{-1}$ *or* $m\,V^{-1}$
Piezoelectric strain	3rd	g_{ijk}	$V\,m\,N^{-1}$ *or* $m^2\,C^{-1}$
Piezoelectric stress	3rd	e_{ijk}	$C\,m^{-2}$ *or* $N\,V^{-1}\,m^{-1}$
Piezoelectric stress	3rd	h_{ijk}	$V\,m^{-1}$ *or* $N\,C^{-1}$

When notation is used as a superscript, it means the value is held constant during measurement.

ourselves to linear physical properties, which are properties that can be described by a linear relationship between cause and effect such as stress and electric field for linear piezoelectricity. Piezoelectricity is a reversible effect, so removing the stress will remove the induced electric field.

Direct and converse effect

The first effect discovered by the Curie brothers was the direct effect. When a mechanical stress is applied to a crystal an electric polarization results. To introduce the effect, we use a simplified situation of constant entropy (adiabatic case) and temperature conditions; other variables not explicitly mentioned are also assumed constant.

The direct effect can be written as the relationship between the 2nd rank stress tensor σ_{ik} and 1st rank electric polarization vector P_i, linked by the piezoelectric tensor d_{ijk} as follows

$$\begin{aligned}P_1 &= d_{111}\sigma_{11} + d_{112}\sigma_{12} + d_{113}\sigma_{13} + d_{121}\sigma_{21} \\ &\quad + d_{122}\sigma_{22} + d_{123}\sigma_{23} + d_{131}\sigma_{31} + d_{132}\sigma_{32} + d_{133}\sigma_{33}, \\ P_2 &= d_{211}\sigma_{11} + d_{212}\sigma_{12} + d_{213}\sigma_{13} + d_{221}\sigma_{21} + d_{222}\sigma_{22} \\ &\quad + d_{223}\sigma_{23} + d_{231}\sigma_{31} + d_{232}\sigma_{32} + d_{233}\sigma_{33}, \\ P_3 &= d_{311}\sigma_{11} + d_{312}\sigma_{12} + d_{313}\sigma_{13} + d_{321}\sigma_{21} + d_{322}\sigma_{22} \\ &\quad + d_{323}\sigma_{23} + d_{331}\sigma_{31} + d_{332}\sigma_{32} + d_{333}\sigma_{33}.\end{aligned}$$

The electric polarization is the electric dipole moment per unit volume, which is proportional to the electric field defined by $P_i = \kappa_0\, \chi_{ij}\, E_j$ where κ_0 is the permittivity of a vacuum (8.854188×10^{-12} C V^{-1} m^{-1}), χ_{ij} is the dielectric susceptibility tensor in F m^{-1} and E_j is the electric field strength in V m^{-1}. We use the more compact tensor notation with the summations presented in the form

$$P_i = \sum_{j=1}^{3}\sum_{k=1}^{3} d_{ijk}\sigma_{jk}, \quad i = 1, 2, 3,$$

involving the implicit Einstein summation convention (i.e. when an index occurs twice in the same term, summation with respect to that index is understood). For example, it is understood that summations occur for indices j and k for the direct effect as they occur twice in d_{ijk} and σ_{ik} on the right-hand side of the equation

$$P_i = d_{ijk}\sigma_{jk},$$

where P_i is electric polarization, d_{ijk} the piezoelectric tensor and σ_{ik} the stress tensor.

The converse effect can be written as

$$\varepsilon_{jk} = \sum_{i=1}^{3} d_{ijk}E_i (j, k = 1, 2, 3) \quad \text{or} \quad \varepsilon_{jk} = d_{ijk}E_i,$$

where ε_{ij} is the elastic strain tensor and E_k is the electric field vector. Here again the summation is understood for the index i occurring in d_{ijk} and E_i. As 1st rank electric polarization P_i and electric field E_k vectors have the index $i = 1,2$ or 3 and 2nd rank stress σ_{ik} and elastic strain ε_{jk} tensors have indices $j = 1,2$ or 3 and $k = 1,2$ or 3, the 3rd rank piezoelectric tensor d_{ijk} has $3 \times 3 \times 3 = 27$ coefficients. The symmetric nature of the stress and strain 2nd rank tensors for linear elasticity results in interchangeability of jk and kj indices of piezoelectric tensor d_{ijk}, which reduces the number of independent components from 27 to 18 where $d_{ijk} = d_{ikj}$ but $d_{ijk} \neq d_{jik}$.

In the literature the tensor d_{ijk} is reported for single crystals in the practical and compact Voigt matrix notation. The conversion from Voigt d_{in} notation to tensor d_{ijk} notation means $d_{ijk} = d_{in}$ when $n = 1, 2, 3$ and $d_{ijk} = \frac{1}{2}d_{in}$ when $n = 4, 5, 6$. The factor of $\frac{1}{2}$ is due to the difference between the strain tensor and 'engineering' shear strains of Voigt matrix notation. The piezoelectric tensor will always have three indices and Voigt matrix notation two indices. The direct and converse effects can also be written in Voigt matrix notation as

$$P_i = \sum_{n=1}^{6} d_{in}\sigma_j, \ i = 1, 2, 3, \quad \text{and}$$

$$\varepsilon_j = \sum_{i=1}^{3} d_{ni}E_i, \ n = 1, 2, 3, 4, 5, 6.$$

Alternatively, we can write the direct and converse effects in reduced matrix notation **bold** type (see Bond 1943; Bishop 1981; Russell & Ghomshei 1997 for tensor examples using the matrix method) or full Voigt matrix and vector notation

$$\boldsymbol{P} = \boldsymbol{d}\boldsymbol{\sigma} = \begin{pmatrix} P_1 \\ P_2 \\ P_3 \end{pmatrix}$$

$$= \begin{pmatrix} d_{11} & d_{12} & d_{13} & d_{14} & d_{15} & d_{16} \\ d_{21} & d_{22} & d_{23} & d_{24} & d_{25} & d_{26} \\ d_{31} & d_{32} & d_{33} & d_{34} & d_{35} & d_{36} \end{pmatrix} \times \begin{pmatrix} \sigma_1 \\ \sigma_2 \\ \sigma_3 \\ \sigma_4 \\ \sigma_5 \\ \sigma_6 \end{pmatrix}$$

$$\boldsymbol{\varepsilon} = \boldsymbol{d}^{\mathrm{T}}\boldsymbol{E} = \begin{pmatrix} \varepsilon_1 \\ \varepsilon_2 \\ \varepsilon_3 \\ \varepsilon_4 \\ \varepsilon_5 \\ \varepsilon_6 \end{pmatrix} = \begin{pmatrix} d_{11} & d_{21} & d_{31} \\ d_{12} & d_{22} & d_{32} \\ d_{13} & d_{32} & d_{33} \\ d_{14} & d_{24} & d_{34} \\ d_{15} & d_{25} & d_{35} \\ d_{16} & d_{26} & d_{36} \end{pmatrix} \begin{pmatrix} E_1 \\ E_2 \\ E_3 \end{pmatrix}.$$

We now write the matrix $\boldsymbol{d}$ in partial differential form and a table format so it is easy to understand

that the direct and converse effects require that the tensor $\boldsymbol{d}$ is in units of Coulomb/Newton and its transpose $\boldsymbol{d}^{\mathrm{T}}$ in units of metre/Volt.

$$\boldsymbol{d} = d_{in} \equiv \frac{\partial \sigma_n}{\partial P_i}$$

$$\equiv \begin{array}{c|cccccc} & \sigma_1 & \sigma_2 & \sigma_3 & \sigma_4 & \sigma_5 & \sigma_6 \\ P_1 & d_{11} & d_{12} & d_{13} & d_{14} & d_{15} & d_{16} \\ P_2 & d_{21} & d_{22} & d_{23} & d_{24} & d_{25} & d_{26} \\ P_3 & d_{31} & d_{32} & d_{33} & d_{34} & d_{35} & d_{36} \end{array}$$

$$\boldsymbol{d}^{\mathrm{T}} = d_{ni} \equiv \frac{\partial E_i}{\partial \varepsilon_n} \equiv \begin{array}{c|ccc} & E_1 & E_2 & E_3 \\ \varepsilon_1 & d_{11} & d_{21} & d_{31} \\ \varepsilon_2 & d_{12} & d_{22} & d_{32} \\ \varepsilon_3 & d_{13} & d_{23} & d_{33} \\ \varepsilon_4 & d_{14} & d_{24} & d_{34} \\ \varepsilon_5 & d_{15} & d_{25} & d_{35} \\ \varepsilon_6 & d_{16} & d_{26} & d_{36} \end{array} .$$

Similar considerations also apply to the other piezoelectric tensors that we introduce later in the section on constitutive equations.

Symmetry and rotation

All crystals that belong to centrosymmetric point groups (i.e. the 11 Laue classes) are piezoelectrically inactive. All crystals belonging to the 21 non-centrosymmetric point groups are piezoelectrically active, with the exception of cubic **432**. In the **432** point group, the presence of four-fold axes parallel to [100], [010] and [001] makes all directions perpendicular to these axes non-polar (Hermann 1934), and results in all tensor coefficients that are non-zero ($d_{14} = d_{25} = d_{36}$) in the two other piezoelectric cubic points groups (**23** and $\bar{\mathbf{4}}$**3m**) being zero in **432**. Hence, there are 20 non-centrosymmetric point groups for piezoelectric active crystals, of which 10 enantiomorphic space group pairs do not have improper rotations (i.e. no mirror planes). Such crystals occur in right-handed and left-handed forms (e.g. α-quartz) and are distributed in 6 point groups (**4**, **422**, **3**, **32**, **6** and **622**). Standard texture orientation determination using diffraction-based measurements that obey Friedel's law can be routinely made for non-enantiomorphic piezoelectric crystals where the diffraction intensity of planes (**hkl**) and ($\bar{\mathbf{h}}\bar{\mathbf{k}}\bar{\mathbf{l}}$) are the same because of the centre of symmetry that is imposed by the diffraction process. To distinguish the right-handed and left-handed forms of enantiomorphic crystals additional information, such as dynamical scattering revealing a violation of Friedel's law (e.g. Goodman & Johnston 1977; Goodman & Secomb 1977; Bunge & Esling 1985; Marthinsen & Høier 1988), is required. Alternatively gyration, also called optical activity, can be used in optically transparent crystals (e.g. Wenk 1985) to detect the handedness of crystal.

Piezoelectric tensors, like all 3rd rank tensors, obey the transformation laws such that $P'_{ijk} = a_{il}a_{jm}a_{kn}P_{lmn}$, where a_{il} etc. are rotation matrices ($a^{\mathrm{T}} = a^{-1}$) that change the orientation of the piezoelectric tensor P_{lmn} to some new orientation in specimen coordinates P'_{ijk}. The application of a rotation that belongs to the point group of the crystal symmetry means that the tensor will be invariant. An orientation in MTEX can typically be defined by Euler angles, quaternions and axis/angle pairs.

For a crystal with point group symmetry **1** there are no intrinsic symmetry rotations or mirror planes that will reduce the number of non-zero coefficients from the 18 of the (3×6) Voigt matrix format of the piezoelectric tensor for a triclinic crystal. If the crystal has higher symmetry, then the number of independent non-zero coefficients is reduced. For example, in the monoclinic point group **2** with a two-fold 180° rotation about either the **b**-axis or the **c**-axis depending on the crystallographic setting, there are only 8 independent non-zero coefficients. With the increasing number of symmetry operations, the number of non-zero coefficients reduces to one for hexagonal $\bar{\mathbf{6}}$**2m** and cubic $\bar{\mathbf{4}}$**3m** and **23** point groups.

The crystal reference frame

Matter tensors describing physical properties such as the piezoelectricity of a single crystal or polycrystalline specimen require a tensor reference frame. In the case of single crystals, the reference frame must be defined with respect to the crystal structure in terms of crystallographic directions, whereas for polycrystalline specimens it must be defined in specimen coordinates. We will restrict ourselves to tensors of single or polycrystals defined in a Cartesian reference frame comprising 3 unit vectors, $\boldsymbol{X}$, $\boldsymbol{Y}$, $\boldsymbol{Z}$. The use of an orthogonal reference frame for single crystals avoids the complications of the metric associated with the crystal unit cell. In any case, almost all modern measurements of physical property tensors are reported using right-handed Cartesian reference frames.

We have previously discussed how the single-crystal tensor reference frame is defined using the crystal coordinate system in Mainprice *et al.* (2011). Here we will illustrate the definition of the crystal symmetry frame in MTEX using the example of a right-handed single crystal of α-quartz.

In MTEX the alignment of the crystal reference frame is defined together with the symmetry group

and the crystal coordinate system. For the case of 3rd rank tensors such as piezoelectricity we need to define the point group symmetry rather than the Laue class, which is sufficient for symmetric 2nd and 4th rank tensors as illustrated in MTEX by Mainprice *et al.* (2011). For example, α-quartz is in Laue class $\bar{3}\mathbf{m}$, which imposes a centre of symmetry it does not have physically; the point group **32** has no centre of symmetry and is compatible with the piezoelectric properties of α-quartz. The information is stored in a variable of type `symmetry`. For example, for α-quartz the point group symmetry is **32**, the axis lengths are $a = b = 4.9134$ Å and $c = 5.4052$ Å, $\alpha = \beta = 90^\circ$ and $\gamma = 120^\circ$. As MTEX recognizes that point group symmetry is **32** and has trigonal symmetry, there is no need to enter the cell angles in `symmetry`. Next comes the definition of the the Cartesian tensor reference frame *X*, *Y*, *Z*, where *X* is parallel to the *a*-axis and *Z* is parallel to *c*-axis.

```
cs_tensor = symmetry('32', 4.9134 4.9134 54052],
'X||a', 'Z||c',...
 'mineral', 'RH alpha - Quartz');

cs_tensor = symmetry (size: 1)
mineral           : RH alpha-Quartz
symmetry          : 32 (-3m)
a, b, c           : 4.9, 4.9, 5.4
alpha, beta, gamma : 90, 90, 120
reference frame   : X||a, Y||b*, Z||c
```

When defining a crystal piezoelectric tensor ***d*** with respect to this crystal reference frame, the variable cs_tensor becomes part of the newly generated tensor object ***d*** and, in this way, the tensor coefficients and the tensor reference frame are stored together. For example, ***d*** defines the piezoelectric tensor ***d*** in pC N^{-1}(where 1 pC = 10^{-12} C) of right-handed α-Quartz. In this case we need to specify DoubleConvention so that MTEX knows that this tensor transforms Voigt to tensor notation as $d_{ijk} = d_{in}$, $n = 1, 2, 3$ and $d_{ijk} = \frac{1}{2}d_{in}$, $n = 4, 5, 6$.

```
% Enter Piezoelectric (strain) tens or
  (d_ij ) as (3 by 6) matrix
% Md line by line in pC/N
% Ogi, H., Ohmori, T. Nakamura, N. and
  Hirao M. (2006)
% RH alpha-quartz  d11 = -1.9222
  d14 = -0.1423
Md =
[[-1.9222 +1.9222 0 -0.1423 0 0];...
   [  0      0      0   0     0 +0.1423 3.8444];...
   [  0      0      0   0     0 0]];
d = tensor (Md,cs_Tensor,'rank',3,
   'propertyname',...
   'piezoelectric_strain_tensor',
   'unit', 'pC/N','
   Double Convention')
```

```
d = tensor (show methods, plot)
propertyname       : piezoelectric strain
                     tensor
unit               : pC/N
rank               : 3 (3 × 3 × 3)
doubleConvention   : true
mineral            : RH alpha-Quartz (32,
                     X||a, Y||b*, Z||c*)

tensor in compact matrix form:
-1.9222  1.9222    0   -0.1423        0        0
      0       0    0         0   0.1423   3.8444
      0       0    0         0        0        0
```

The transformation from Voigt to tensor notation and vice versa is discussed in more detail later in the section on constitutive equations.

Longitudinal surfaces and other representations of tensors

The single-crystal piezoelectric tensor can be visualized in several ways. The base of all visualizations is the value of the tensor ***d*** in a direction ***x***, or dvalue (***x***) which is given by

$$\text{dvalue}(\boldsymbol{x}) = x_i x_j x_k d_{ijk}.$$

To compute the dvalue (***x***) in MTEX we first need to define a direction relative to the tensor reference frame. This is done by the command `Miller`. The following syntax is supported

- by coordinates with respect to the Euclidean crystal reference frame *X*, *Y*, *Z*

  ```
  x = Miller (1, 0, 0, 'xyz', cs_tensor)
  ```

- by coordinates with respect to the crystal directions *a*, *b*, *c*

  ```
  x = Miller (1, 0, 0, 'uvw', cs_tensor)
  ```

- by coordinates with respect to the reciprocal coordinate system *a**, *b**, *c**

  ```
  x = Miller (1, 0, 0, 'hkl', cs_tensor)
  ```

- by polar coordinates

  ```
  x = Miller (polar_angle,
      azimuth_angle,'polar', cs_tensor)
  ```

Note that again the variable `cs_tensor` is passed on to the definition of the direction to make clear that the coordinates are given with respect to this specific reference frame. Now we can use the command `directionMagnitude` to compute dvalue (***x***).

```
dvalue = directionalMagnitude(d, Miller
   (1, 0, 0, 'xyz', cs_tensor))
dvalue = -1.9222
```

With vector3d $\mathbf{x}$ = vector3d(1,0,0), the result is -1.9222 pC N^{-1} as expected for a positive a-axis when $X \parallel a$; for vector3d(0.5,0.8660,0) it is 1.9222 pC N^{-1} as expected for a negative a-axis. For the direction vector3d(0,0,1) parallel to the c-axis, the value for **d** is zero as this is not a polar direction.

```
% positive a-axis (1.0, 0.0, 0.0)
positive_a_axis = xvector
dvalue = directionalMagnitude(d,xvector)
dvalue = -1.9222
% alternative use uvtw = +a1 [2, -1, -1, 0]
dvalue = directionalMagnitude
 (d, vector3d (Miller(2, -1, -1, 0,
   cs_Tensor, 'uvw')))
polar_angle = 90* degree
azimuth_angle = 60* degree
negative_a_axis = vector3d ('polar',
polar_angle, azimuth_angle)
dvalue = directionalMagnitude
 (d, negative_a_axis)
dvalue = 1.9222
% alternative use uvtw = -a [1, 1, -2, 0]
dvalue = directionalMagnitude (d, vector3d
 (Miller (1, 1, -2, 0, cs_Tensor, 'uvw')))
```

Perhaps the most classical representation of piezoelectricity is the longitudinal surface. The longitudinal surface of infinitesimal area is normal to an axial tensile stress parallel to x_1'. The polarization normal to the surface is given by $P_1' = d_{111}' \sigma_{11}'$, and d_{111}' is the polarization value parallel to x_1' for unit stress. The longitudinal surface is defined by the radius vector **r** parallel to the direction x_1', which was previously in the orientation x_1.

$$\boldsymbol{r} = d_{111}' = a_{1i}a_{1j}a_{1k}d_{ijk} \quad \text{or}$$
$$\boldsymbol{r} = d_{222}' = a_{2i}a_{2j}a_{2k}d_{ijk} \quad \text{or}$$
$$\boldsymbol{r} = d_{333}' = a_{3i}a_{3j}a_{3k}d_{ijk}$$

From this expression we can understand that radius vector **r** is rotated in the *XYZ* tensor frame to map the longitudinal surface, where $\boldsymbol{r} = d_{111}' = \text{dvalue}(\boldsymbol{x})$ (Fig. 1).

The surface can be plotted in a 2D section normal to any direction defined by MTEX vector3d in the tensor coordinate frame. For example, to plot the surface in the basal (0001) plane we use the predefined zvector = vector3d(0,0,1) as $Z \parallel c$, and plot the plane normal to the predefined yvector = vector3d(0,1,0), which is a 1st order prism plane (m) containing the a- and c-axes in Figure 2. Using the MTEX plot command with the option 'section' allows us to plot the 2D longitudinal surface, which is the limiting surface between positive and negative values of the tensor ***d***. In regions outside these longitudinal limiting surfaces, no polarization is possible.

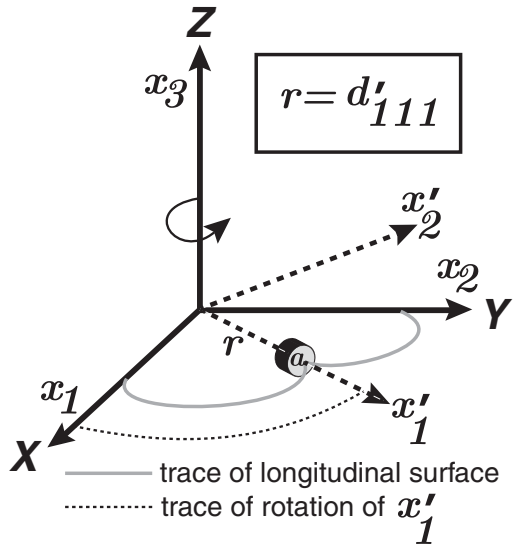

Fig. 1. Construction of the longitudinal surface by the rotation of x_1' about the **Z** axis with $d_{111}' = \text{dvalue}(\boldsymbol{x})$; **a** represents the infinitesimal surface area.

```
plot (d, 'section', zvector)
% alterative use uvtw = c [0, 0, 0, 1]
Plot (d, 'section', vector3d (Miller
 (0, 0, 0, 1, cs_Tensor, 'uvw'))
plot (d, 'section', yvector)
% alterative use uvtw = m[0,1, -1, 0]
Plot (d, 'section', vector3d (Miller
 (0, 1, -1, 0, cs_Tensor, 'uvw'))
```

In MTEX the magnitude of a piezoelectric tensor can be plotted as a function of crystal direction in the tensor frame on an equal-area stereogram, as the crystallographic asymmetric unit, the complete hemisphere or as upper and lower hemispheres. The plot of both hemispheres shows the 3D distribution of the piezoelectric tensor ***d*** values in pC N^{-1}, where the maximum negative value (white) is parallel to the three $+a$-axes and the value parallel to the c-axis is zero Figure 3. The upper and lower hemisphere distributions are identical.

```
plot (d, 'complete')
colorbar
annotate ([xvector, yvector, zvector],
 'label',...
{'X||a', 'Y||m', 'Z||c', 'backgroundcolor',
 'w', 'FontSize', 18);
```

To better understand the distribution of the piezoelectric tensor ***d*** a perspective 3D plot can be used which can be rotated interactively using the command rotate3d in the Matlab environment. Figures 4 and 5 are generated using the command plot, illustrated for α-quartz (Fig. 4) and sphalerite (ZnS), also know as zincblende (Fig. 5). Sphalerite is an

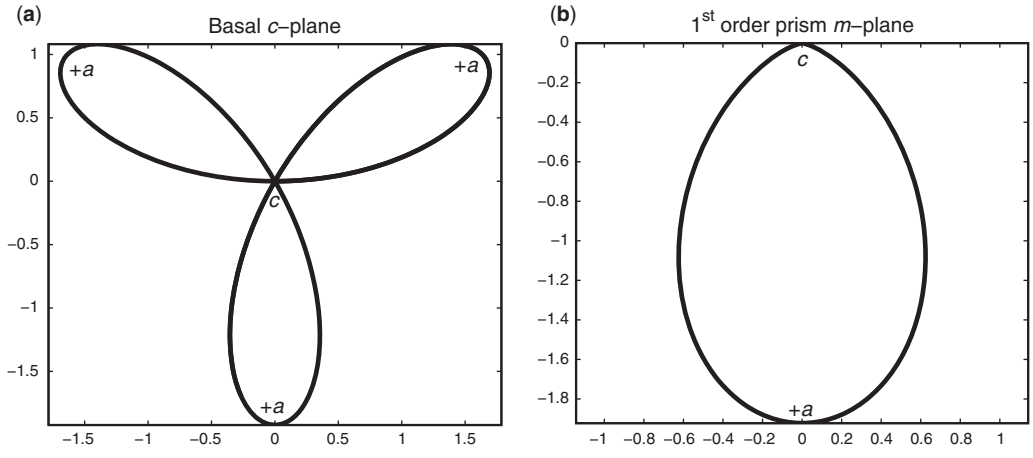

Fig. 2. Plot of longitudinal surfaces of the piezoelectric tensor ***d*** for right-handed α-quartz **32**: (**a**) basal plane (c); and (**b**) 1st order prism plane (m). Units pC N^{-1}.

important mineral in zinc-bearing mining deposits (e.g. Bishop & Emerson 1999). The symmetry of sphalerite is cubic $\bar{4}$**3m** point group, where the only non-zero independent value of tensor ***d*** is d_{14} and the other three non-zero coefficients are $d_{14} = d_{25} = d_{36}$. The $\bar{4}$**3m** point group has a set of 24 symmetry operations, but no proper (rotational) four-fold axis and only four-fold inversion axes parallel to the a, b and c-axes.

```
% crystal symmetry ( c s )
cs_tensor = symmetry (' - 43m',
 [5.41 5.41 5.41],...
 [90.0000 90.000 90.000]* degree,
'X|| a', 'Z|| c', 'mineral', 'Sphalerite')
%
% Enter Piezoelectric (strain) tensor
 (d_ij) as (3 by 6) matrix
% Md line by line in pC/N
% Berlincourt, D., Jaffe, H., and
  Shiozawa, L.R. (1963)
% Physical Review 129, 1009 - 1017.
% Sphalerite (ZnS) d14 = 3.180 pC/N
Md = [ [ .00 .00 .00  3.18  .00  .00 ];...
     [  .00 .00 .00   .00 3.18  .00 ];...
     [  .00 .00 .00   .00  .00 3.18 ] ];
```

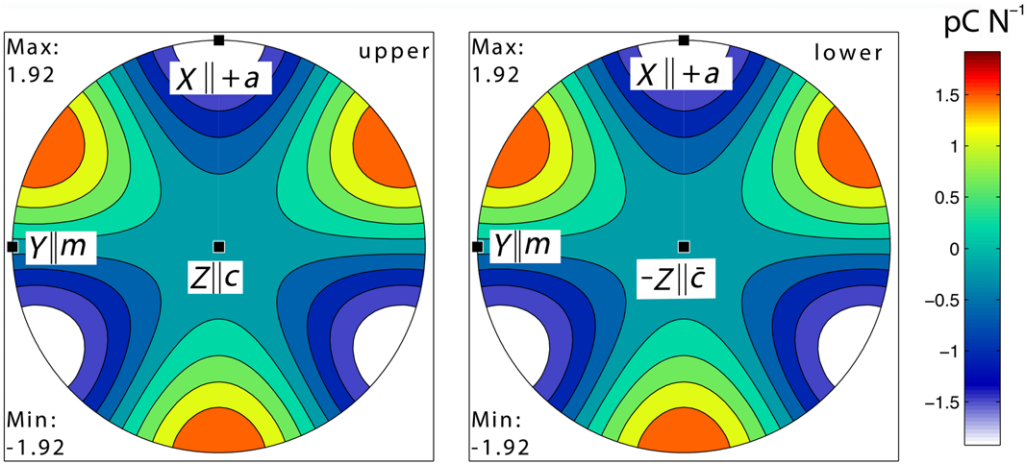

Fig. 3. Upper and lower hemisphere plots of the piezoelectric tensor ***d*** for right-handed α-quartz **32**: using the 'complete' option with default filled contour option and the MTEX annotate command.

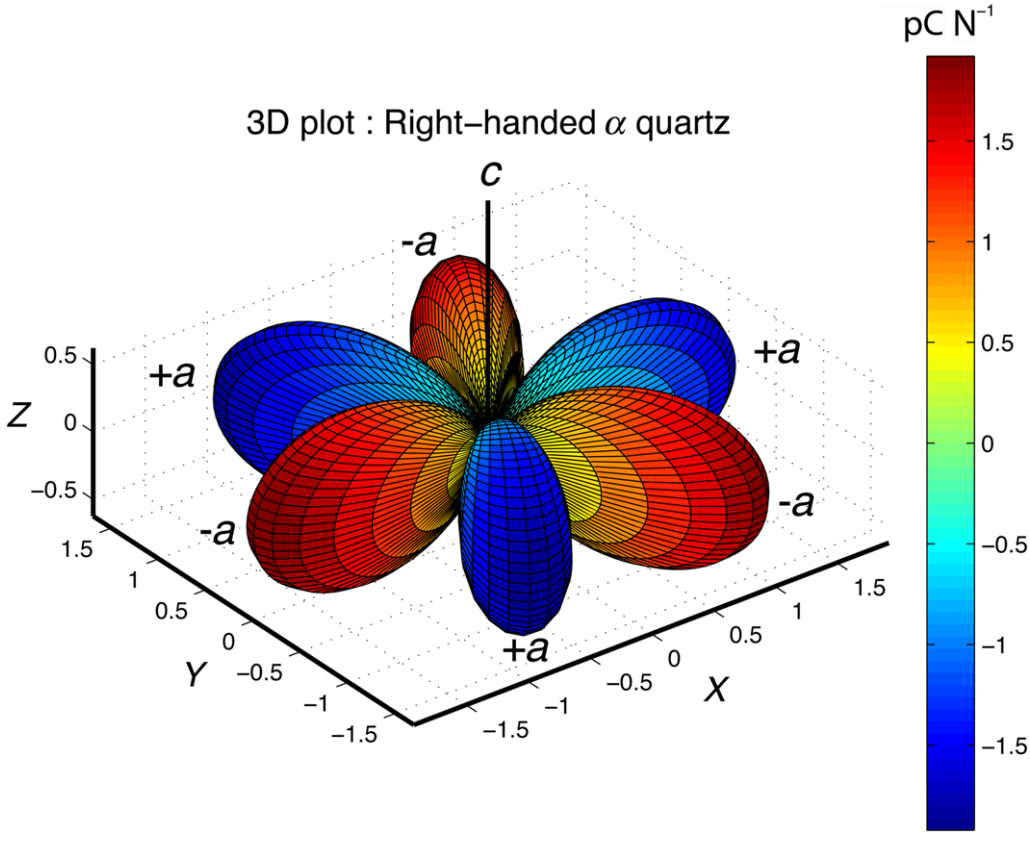

Fig. 4. 3D plot of the piezoelectric tensor ***d*** for right-handed α-quartz **32** using plot(d, '3D'). Note the three-fold c-axis repeating the red (positive) and blue (negative) lobes, two-fold a-axes, $+a$-axes have negative values and the zero value along the c-axis.

```
d = tensor (Md,cs_Tensor, 'rank', 3,
    'propertyname',...
    'piezoelectric_strain_tensor',
    'unit','pC/N', 'DoubleConvention')
% plot
plot (d, '3d')
% activate MATLAB 3d interactive rotation
   of plot
rotate3d

cs_tensor = crystal symmetry
    (show methods, plot)

  mineral   : Sphalerite
  symmetry  : -43m (m - 3m)

d = tensor (show methods, plot)
  propertyname        : piezoelectric
                        strain tensor
  unit                : pC/N
  rank                : 3 (3 × 3 × 3)
  doubleConvention    : true
  mineral             : Sphalerite (-43m)

tensor in compact matrix form:
 0  0  0  3.18     0     0
 0  0  0     0  3.18     0
 0  0  0     0     0  3.18
```

Finally, we should point out that for two crystal symmetry point groups **422** and **622** there is no longitudinal effect; in these two groups there is only one independent piezoelectric coefficient d_{14}. If we write out the full equation for the long longitudinal effect for these symmetry groups we have, in tensor notation,

$$d'_{111} = a_{11}a_{12}a_{13}2d_{123} + a_{12}a_{11}a_{13}2d_{213}$$

and in Voigt notation

$$d'_{11} = a_{11}a_{12}a_{13}(d_{14} + d_{25}).$$

In these symmetry groups, $d_{14} = -d_{25}$ such that $d'_{11} = 0$. Hence, no longitudinal effect and no

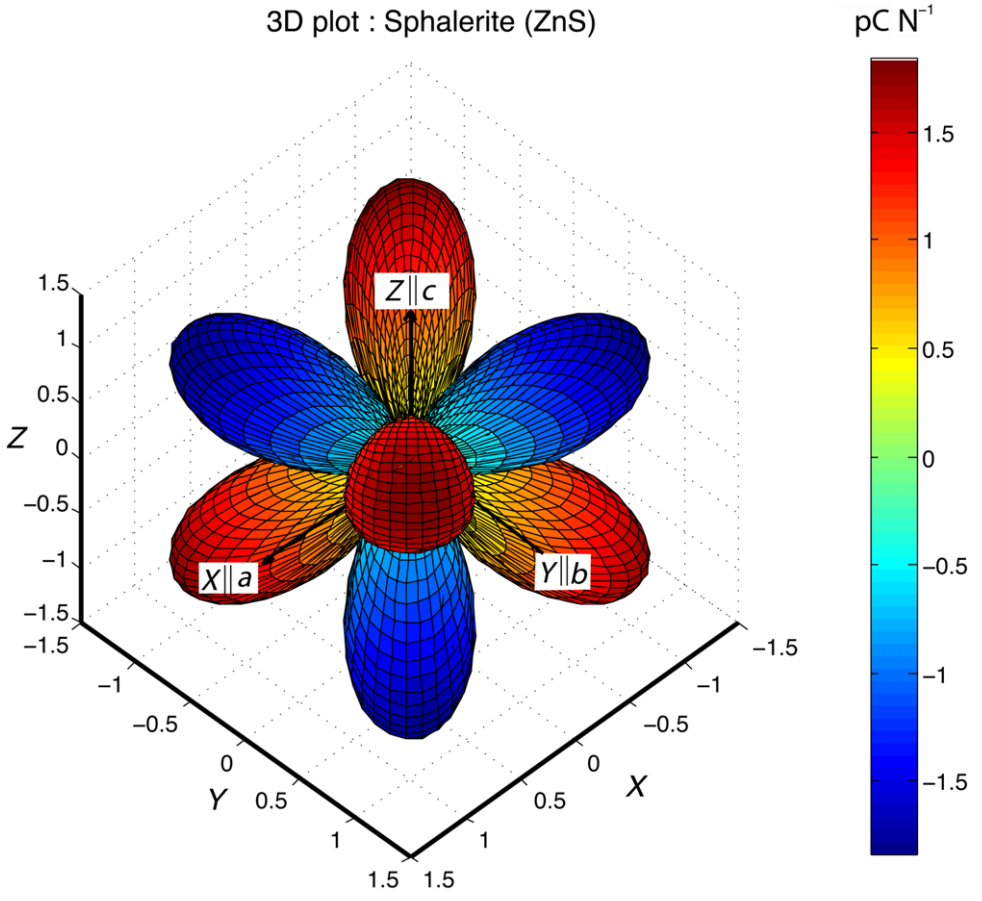

Fig. 5. 3D plot of the piezoelectric tensor ***d*** Sphalerite $\bar{4}3\mathbf{m}$ using plot(d,'3D'). Note the three-fold [111] cube axes repeating the red (positive) and blue (negative) lobes and two-fold axes along *a*, *b* and *c*.

polar axes are present, and electric polarization can only be generated by shear. Two examples are β-quartz point group **622**, $d_{14} = -1.86$ pC N^{-1} (about two times that of α-quartz) at 612 (Cook & Weissler 1950) and paratellurite (α-TeO_2) point group **422**, $d_{14} = 12.41$ pC N^{-1} (Ogi *et al.* 2004).

Hydrostatic effect

The hydrostatic effect is simply described by the direct piezoelectic effect, where the electric field is considered to be constant and the D vector of electric displacement is equal to the polarization P so that

$$P_i = D_i = d_{ijk}\sigma_{jk}.$$

The hydrostatic pressure p is given by $\sigma_{jk} = -p\delta_{jk}$, where δ_{jk} is the Kronecker delta:

$$P_i = -d_{ikk}p.$$

The hydrostatic effect is conveniently defined by the three orthogonal components parallel to tensor frame X, Y, Z in Voigt matrix notation. In Voigt matrix notation, components related to normal stresses are d_{in} (where $i = 1, 2, 3$ and $n = 1, 2, 3$) and those that involve shear stresses d_{in} (where $i = 1, 2, 3$ and $n = 4, 5, 6$). Obviously only the coefficients related to normal stress are compatible with hydrostatic stress.

$$P_1 = -(d_{11} + d_{12} + d_{13})p$$
$$P_2 = -(d_{21} + d_{22} + d_{23})p$$
$$P_3 = -(d_{31} + d_{32} + d_{33})p.$$

The hydrostatic piezoelectric coefficient (Tichý *et al.* 2010) is defined as scalar in the fixed single-crystal X, Y and Z tensor co-ordinate frame

$$d_h = (d_{11} + d_{12} + d_{13}) + (d_{21} + d_{22} + d_{23}) + (d_{31} + d_{32} + d_{33}),$$

where d_h has to be a non-zero value after taking into account the action of symmetry on the signs and magnitudes of d_{in}. The hydrostatic effect is only present in 10 crystal point groups (**$\bar{1}$**, **2**, **m**, **mm2**, **4**, **4mm**, **3**, **3m**, **6**, **6mm**) out of 20 for piezoelectric crystals. For 7 crystal point groups the hydrostatic polarization only occurs along the *c*-axis direction (Klapper & Hahn 2006). After symmetry of the tensor is taken into account, this requires that

$$d_h = 2d_{31} + d_{33}$$

for (**4**, **4mm**, **3**, **3m**, **6**, **6mm**) and

$$d_h = d_{31} + d_{32} + d_{33}$$

for (**mm2**). For point group (**2**) with two-fold symmetry and the hydrostatic effect along the *b*-axis,

$$d_h = d_{21} + d_{22} + d_{23}.$$

For point group (**m**) with two-fold symmetry along the *b*-axis and hydrostatic effect along [*u*0*w*] directions,

$$d_h = (d_{11} + d_{12} + d_{13}) + (d_{31} + d_{32} + d_{33}).$$

For point group (**$\bar{1}$**), all directions [*uvw*] are possible:

$$d_h = (d_{11} + d_{12} + d_{13}) + (d_{21} + d_{22} + d_{23}) + (d_{31} + d_{32} + d_{33}).$$

The only common minerals exhibiting the hydrostatic effect are the tourmaline group (**3m**), wurtzite group (**6mm**), oxides with perovskite structure and all minerals that are pyroelectric, as the same symmetry constraints apply. The presence of pressure in almost all geological situations could potentially generate electrical polarization if piezoelectric minerals are present. However, relatively few minerals exhibit the hydrostatic effect. Some special situations may occur in zinc-bearing mining deposits where two piezoelectric polymorphs of ZnS, sphalerite (**43m**) without a hydrostatic effect and wurtzite (**6mm**) with a hydrostatic effect are often associated. It is also interesting to note that several common sulphide ore minerals – bismuthinite (Bi_2S_3 **mm2**), chalcocite (Cu_2S **2/m**), pyrrhotite ($Fe_{(1-x)}S_x$ **6/mmm**) and stibnite (Sb_2S_3 **mm2**) – are ferroelectric (Corry 1994), of which bismuthinite and stibnite occur in piezoelectric point groups. The piezoelectric effect has been used extensively in geophysical exploration for the mining industry in Russia (Neishtadt *et al.* 2006). The hydrostatic effect has many industrial applications such as pressure measurement and underwater sonar (historically, tourmaline has been used in sonar devices). We use the tensor coefficients recently measured for tourmaline (Pandey & Schreuer 2012) to illustrate the calculation of d_h. Tourmaline has symmetry **3m**, in which the only non-zero coefficients involving normal stresses are d_{21}, d_{22}, d_{31}, d_{32} and d_{33} and where by symmetry $d_{21} = -d_{22}$, such that their combined effect is zero. The remaining non-zero terms are $d_h = d_{31} + d_{32} + d_{33} = 0.16 + 0.16 + 1.91 = 2.23$ pC N^{-1}.

Constitutive equations

Constitutive equations define the coupling between independent variables. To visualize the relationships between different variables of electric field $\boldsymbol{E}$, electric displacement $\boldsymbol{D}$, strain $\boldsymbol{\varepsilon}$, stress field $\boldsymbol{\sigma}$, temperature $\boldsymbol{T}$ and entropy $\boldsymbol{S}$, Heckmann (1925) introduced a triangular diagram (Fig. 6a). From this triangular diagram we have chosen the four variables stress, strain, electric field and electric displacement associated with piezoelectricity. This is equivalent to setting the variables entropy and temperature to constant values for the constitutive equations we have chosen to present. The constitutive or coupled equations given below are taken from Mason (1966); other equations are given by Ikeda (1990). A pair of constitutive equations is required to describe the mechanical and electrical behaviour of a piezoelectric crystal. The equations are given in tensor and matrix notation as **bold** characters. In matrix notation the superscript T means transposed. Superscripts $\boldsymbol{E}$, $\boldsymbol{D}$, $\boldsymbol{\varepsilon}$ and $\boldsymbol{\sigma}$ signify that these variables are held constant during the measurement of the tensor. For example, in the first pair of equations we have s^E_{ijkl} which is the elastic compliance tensor measured at constant electric field, and κ^σ_{ik} which is the dielectric permittivity at constant stress. The first pair of constitutive equations below illustrate the role of piezoelectric strain coupling to electric field with the piezoelectric tensor d. We have on the right-hand side the variables associated with mechanical stress σ and electric field $\boldsymbol{E}$ in both equations. On the left-hand side, we have the resulting values of elastic strain ε and electric displacement $\boldsymbol{D}$. These equations are therefore called the Strain-Electric displacement equations. In the first equation, the first and second terms on the right-hand side are the stress and the electric field contributions to the elastic strain. The second term is the piezoelectric converse coupling effect. In the second equation, the first and second terms on the right-hand side are the stress and electric field contributions to electric displacement. The first term is the piezoelectric direct coupling effect and the second term is the classical relation for electric displacement of a dielectric crystal. The same

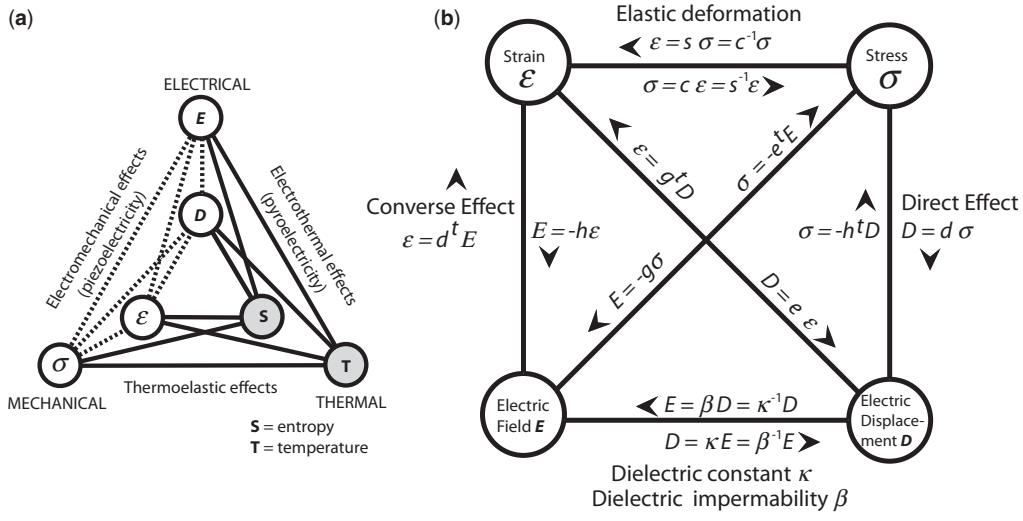

Fig. 6. Interactions between variables. (**a**) The Heckmann triangle shows the complete set of thermodynamical variables. The variables chosen for constitutive equations are in the white circles and the constant variables (entropy and temperature) in circles with grey shading. (**b**) The interaction square with strain, stress, electric displacement and electric field variables at constant entropy and temperature. The piezoelectric tensors ***d***, ***e***, ***g*** and ***h*** in the direct effect are marked with downward arrows and in the converse effect by upward arrows.

logic applies to the other pairs of equations as follows.

(1) Piezoelectric strain to electric field coupling or Strain-Electric displacement equations with 'strain' piezoelectric tensor d can be written:

$$\varepsilon_{ij} = s^{E}_{ijkl}\sigma_{kl} + d_{kij}E_k, \quad \boldsymbol{\varepsilon} = \mathbf{s}^{\mathbf{E}}\boldsymbol{\sigma} + (\boldsymbol{d})^{\mathrm{T}}\boldsymbol{E}$$

$$D_i = d_{ijk}\sigma_{ij} + \kappa^{\sigma}_{ik}E_k, \quad \boldsymbol{D} = \boldsymbol{d}\boldsymbol{\sigma} + \boldsymbol{\kappa}^{\boldsymbol{\sigma}}\boldsymbol{E}$$

(2) Alternatively, piezoelectric stress to electric field coupling or Stress-Electric displacement equations with 'stress' piezoelectric tensor ***e*** can be written:

$$\sigma_{ij} = c^{E}_{ijkl}\varepsilon_{kl} - e_{kij}E_k, \quad \boldsymbol{\sigma} = \boldsymbol{c}^{\boldsymbol{E}}\boldsymbol{\varepsilon} - \boldsymbol{e}^{\boldsymbol{T}}\boldsymbol{E}$$

$$D_i = e_{ijk}\varepsilon_{kl} + \kappa^{\varepsilon}_{ik}E_k, \quad \boldsymbol{D} = \boldsymbol{e}\boldsymbol{\varepsilon} + \boldsymbol{\kappa}^{\boldsymbol{\varepsilon}}\boldsymbol{E}$$

(3) Piezoelectric electric field to stress coupling or Strain-Electric field equations with 'strain' piezoelectric tensor g can be written:

$$\varepsilon_{ij} = s^{D}_{ijkl}\sigma_{kl} + g_{kij}D_k, \quad \boldsymbol{\varepsilon} = \boldsymbol{s}^{\boldsymbol{D}}\boldsymbol{\sigma} + (\boldsymbol{g})^{\mathrm{T}}\boldsymbol{D}$$

$$E_i = -g_{ijk}\sigma_{jk} + \beta^{\sigma}_{ik}D_k, \quad \boldsymbol{E} = -\boldsymbol{g}\boldsymbol{\sigma} + \boldsymbol{\beta}^{\boldsymbol{\sigma}}\boldsymbol{D}$$

(4) Piezoelectric electric field to strain coupling or Stress-Electric field equations with 'stress' piezoelectric tensor h can be written:

$$\sigma_{ij} = c^{D}_{ijkl}\varepsilon_{kl} - h_{kij}D_k, \quad \boldsymbol{\sigma} = \boldsymbol{c}^{\boldsymbol{D}}\boldsymbol{\varepsilon} - (\boldsymbol{h})^{\mathrm{T}}\boldsymbol{D}$$

$$E_i = -h_{ijk}\varepsilon_{kl} + \beta^{\varepsilon}_{ik}D_k, \quad \boldsymbol{E} = -\boldsymbol{h}\boldsymbol{\varepsilon} + \boldsymbol{\beta}^{\boldsymbol{\varepsilon}}\boldsymbol{D}$$

Now we have a set of four piezoelectric tensors – ***d***, ***e***, ***g*** and ***h*** – that form two related sets (***d***, ***g***) and (***e***, ***h***). An illustration of their roles in the direct and converse effects is given by the square diagram in Figure 6b. We can see also the relation between ***d*** and ***g*** by writing them in a differential form with the direct effect first and the converse second. Such representation makes it clear that both are related in the direct effect to $\partial\sigma$ and in the converse effect to $\partial\varepsilon$. The differential form of the tensors is given by

$$d_{ijk} = +\left(\frac{\partial D_i}{\partial \sigma_{jk}}\right)_E = +\left(\frac{\partial \varepsilon_{jk}}{\partial E_i}\right)_\sigma$$

$$g_{ijk} = -\left(\frac{\partial E_i}{\partial \sigma_{jk}}\right)_D = +\left(\frac{\partial \varepsilon_{jk}}{\partial D_i}\right)_\sigma.$$

Secondly, ***e*** and ***h*** are both related in the direct effect in the first relationship to $\partial\varepsilon$ and in the converse effect in the second relationship to $\partial\sigma$

$$e_{ijk} = +\left(\frac{\partial D_i}{\partial \varepsilon_{jk}}\right)_E = -\left(\frac{\partial \sigma_{jk}}{\partial E_i}\right)_\varepsilon$$

$$h_{ijk} = -\left(\frac{\partial E_i}{\partial \varepsilon_{jk}}\right)_D = -\left(\frac{\partial \sigma_{jk}}{\partial D_i}\right)_\varepsilon.$$

The close relation of these two sets of equations is also important for understanding their transformation between the Voigt matrix and tensor notation

and vice versa. The transformation from three-indices to two-indices for the tensors d_{ijk} and g_{ijk} is

$$d_{ijk} = d_{in} \text{ and } g_{ijk} = g_{in}$$
$$\text{with } i, j, k = 1, 2, 3$$
$$\text{when } j = k,\ n = 1, 2 \text{ or } 3$$

$$d_{ijk} = \frac{1}{2} d_{in} \text{ and } g_{ijk} = \frac{1}{2} g_{in}$$
$$\text{with } i, j, k = 1, 2, 3$$
$$\text{when } j \neq k,\ n = 4, 5 \text{ or } 6$$

and the transformation from two-indices to three-indices for the tensors d_{ijk} and g_{ijk} is

$$d_{in} = d_{ijk} \text{ and } g_{in} = g_{ijk}$$
$$\text{with } i, j, k = 1, 2, 3$$
$$\text{when } j = k,\ n = 1, 2 \text{ or } 3$$

$$d_{in} = 2d_{ijk} \text{ and } g_{in} = 2g_{ijk}$$
$$\text{with } i, j, k = 1, 2, 3$$
$$\text{when } j \neq k,\ n = 4, 5 \text{ or } 6$$

where for d_{ijk} and g_{ijk} the factor $\frac{1}{2}$ or 2 is due to the conversions from Voigt matrix shear strain to tensor strains or vice versa. These transformations are activated in MTEX by the option `DoubleConvention` in the tensor command.

The transformation from three-indices to two-indices for the tensors e_{ijk} and h_{ijk} is

$$e_{ijk} = e_{in} \text{ and } h_{ijk} = h_{in}, \quad i, j, k = 1, 2, 3 \quad n = 1, 2, 3, 4, 5, 6$$

and for transformation from two-indices to three-indices for the tensors e_{ijk} and h_{ijk} is

$$e_{in} = e_{ijk} \text{ and } h_{in} = h_{ijk}, \quad i, j, k = 1, 2, 3 \quad n = 1, 2, 3, 4, 5, 6$$

where for e_{ijk} and h_{ijk} there are no correction factors. These transformations are activated in MTEX by the option `SingleConvention` in the tensor command.

The relationship between all $\boldsymbol{d}$, $\boldsymbol{e}$, $\boldsymbol{g}$ and $\boldsymbol{h}$ tensors provides a route for calculating one type of piezoelectric tensor from another, as it is rare that publications quote coefficients of all four piezoelectric tensors.

$$d_{nkl} = e^{\sigma}_{mn} g_{mkl} = e_{nij} s^{E}_{ijkl} \quad \boldsymbol{d} = \boldsymbol{e^{\sigma} g} = \boldsymbol{e s^{E}}$$
$$e_{nkl} = e^{\varepsilon}_{mn} h_{mkl} = d_{nij} c^{E}_{ijkl} \quad \boldsymbol{e} = \boldsymbol{e^{\varepsilon} h} = \boldsymbol{d c^{E}}$$
$$g_{nkl} = \beta^{\sigma}_{mn} d_{mkl} = h_{nij} s^{D}_{ijkl} \quad \boldsymbol{g} = \boldsymbol{\beta^{\sigma} d} = \boldsymbol{h s^{D}}$$
$$h_{nkl} = \beta^{\varepsilon}_{mn} e_{mkl} = g_{nij} c^{D}_{ijkl} \quad \boldsymbol{h} = \boldsymbol{\beta^{\varepsilon} e} = \boldsymbol{g c^{D}}$$

Standards for piezoelectric crystal properties

Over the years various conventions for the signs of physical properties of piezoelectric crystals have been proposed for crystals such as α-quartz, which has left- and right-handed forms. The best known conventions are the International Radio Engineers (IRE) standard published in 1949 (Brainerd *et al.* 1949) and the more recent Institute of Electrical and Electronic Engineering (IEEE) ANSI-IEEE 176 standard published in 1988 (http://www.ieee.org). Both are considered important industrial standards but, as can been seen from Table 1, the sign conventions for elastic and piezoelectric tensors for α-quartz are different. Table 2 provides the values for right- and left-handed α-quartz given in the IRE 1949 standard. If we know the values for d_{ijk} and c^{E}_{ijkl} from Table 2, then we can calculate the coefficients for the other piezoelectric tensors ($\boldsymbol{e}$, $\boldsymbol{g}$ and $\boldsymbol{h}$) in a self-consistent way using the relationships given above starting with $e_{nkl} = d_{nij} c^{E}_{ijkl}$.

In tensor notation this reduces approach to two independent non-zero coefficients for α-quartz with

Table 2. *Conventions for the signs of constants in right- and left-handed α-quartz (simplfied after Tichý* et al. *2010).*

Property	IRE 1949 RH-Quartz	IRE 1949 LH-Quartz	IEEE 1978 RH-Quartz	IEEE 1978 LH-Quartz
Elastic compliance tensor s_{14}	+	+	−	−
Elastic stiffness tensor c_{14}	−	−	+	+
Piezoelectric strain tensor d_{11}	−	+	+	−
Piezoelectric strain tensor d_{14}	−	+	−	+
Piezoelectric stress tensor e_{11}	−	+	+	−
Piezoelectric stress tensor e_{14}	+	−	+	−

Note that all constants are measured in a right-handed Cartesian coordinate system. According to Le Page *et al.* (2002), right-handed α-quartz $c_{14} = -19.7$ GPa.

Table 3. *Properties of α-quartz according to IRE 1949 standard. Original data on* e_{ij}, c^E_{ij}, *and* κ^σ_{ij} *from Ogi* et al. *(2006)*

c^E_{ij} GPa	$d_{ij}\ 10^{-12}$ C N^{-1}	g_{ij} m^2 C^{-1}	e_{ij} C m^{-2}	h_{ij} 10^9 N C^{-1}	κ^σ_{ij} 10^{-12} mf^{-1}
Right-handed α-quartz					
$c^E_{11} = 86.76$	$d_{11} = -1.9222$	$g_{11} = -0.0481$	$e_{11} = -0.1510$	$h_{11} = -3.8512$	$\kappa^\sigma_{11} = 39.17$
$c^E_{12} = 6.868$	$d_{14} = -0.1423$	$g_{14} = -0.0036$	$e_{14} = +0.0610$	$h_{14} = +1.5558$	$\kappa^\sigma_{33} = 41.01$
$c^E_{13} = 11.85$					
$c^E_{14} = -18.02$					
$c^E_{33} = 105.46$					
$c^E_{44} = 58.14$					
Left-handed α-quartz					
$c^E_{11} = 86.76$	$d_{11} = +1.9222$	$g_{11} = +0.0481$	$e_{11} = +0.1510$	$h_{11} = +3.9820$	$\kappa^\sigma_{11} = 39.17$
$c^E_{12} = 6.868$	$d_{14} = +0.1423$	$g_{14} = +0.0036$	$e_{14} = -0.0610$	$h_{14} = -1.9778$	$\kappa^\sigma_{33} = 41.01$
$c^E_{13} = 11.85$					
$c^E_{14} = -18.02$					
$c^E_{33} = 105.46$					
$c^E_{44} = 58.14$					

point group symmetry **32**

$$e_{111} = d_{111}(c^E_{1111} - c^E_{1122}) + 2d_{123}c^E_{1123} = e_{11},$$
$$e_{123} = d_{111}c^E_{1123} + d_{122}c^E_{2223} + 2(d_{123}c^E_{2323}) = e_{14}.$$

In Voigt matrix notation, this can be written

$$e_{11} = d_{11}(c^E_{11} - c^E_{12}) + d_{14}c^E_{14}, e_{14}$$
$$= d_{11}c^E_{14} + d_{12}c^E_{24} + d_{14}c^E_{44}.$$

Similarly, for the g_{nkl} tensor we can write

$$g_{nkl} = \beta^\sigma_{mn}d_{nkl},$$

where β^σ_{mn} is the inverse of κ^σ_{mn} given in Table 1, so that

$$g_{111} = (\kappa^\sigma_{11})^{-1}d_{111} = g_{11},$$
$$g_{123} = (\kappa^\sigma_{11})^{-1}d_{123} = g_{14}/2.$$

For the tensor $h_{nkl} = \beta^\varepsilon_{mn}e_{nkl}$, although we do not have a value for $\varepsilon^\varepsilon_{mn}$ in Table 3, we can calculate the necessary correction from

$$\kappa^\sigma_{mn} - \kappa^\varepsilon_{mn} = d_{nkl}e_{mkl},$$

where

$$\kappa^\sigma_{11} - \kappa^\varepsilon_{11} = 0.57 \times 10^{-12}\,\mathrm{mf}^{-1},$$

which gives $\kappa^\varepsilon_{11} = 39.74 \times 10^{-12}\mathrm{mf}^{-1}$ and hence

$$h_{111} = (\kappa^\varepsilon_{11})^{-1}e_{111} = h_{11},$$
$$h_{123} = (\kappa^\varepsilon_{11})^{-1}e_{123} = h_{14}.$$

Using this method, we have checked the coherency of the sign conventions of the IRE 1949 and IEEE 1987 standards for the four piezoelectric tensors. Both are internally consistent and in agreement with the equations given above. A further consistency check was made by Le Page *et al.* (2002) on the sign of the elastic stiffness coefficient c_{14} for right-handed α-quartz using *ab initio* methods and they found that the sign was negative, which can only be consistent with the IRE 1949 standard (Table 2). We have therefore decided to use the IRE 1949 standard in this paper, together with the most recent published values of piezoelctric tensors for α-quartz by Ogi *et al.* (2006).

Elastic wave propagation

For wave propagation in an infinite elastic piezoelectric medium the appropriate independent variables are the strain (ε) and the electric field (E), which define the constitutive equations coupling the elastic (acoustic) and electromagnetic waves caused by a mechanical vibration. This choice of constitutive equations is sometimes called the piezoelectric stress equations due to the presence of the e_{ijk} tensor. There are five plane-wave coupled solutions in a piezoelectric medium: three elastic

and two electromagnetic (e.g. Auld 1990). Detailed analysis shows that the effects of piezoelectric coupling of elastic and electromagnetic planes waves in infinite media are negligible in comparison with the influence of the quasi-static electric field. The velocity of elastic (acoustic) waves is approximately five orders of magnitude lower than electromagnetic waves. It is therefore only the quasi-static part of the electric field that affects the propagation of elastic waves. The quasi-static electric approximation neglects the rotational part (i.e. the magnetic field B part) of the electromagnetic field ($-\nabla \times E = \partial B/\partial t = 0$ and $-\nabla \cdot E = \rho/\varepsilon_0$ where t is time, ρ is total charge density and ε_0 is permittivity of a vacuum) and retains only the scalar electric field ($E = -\nabla\Phi$, where Φ is the electric potential). The quasi-static electric approximation introduces insignificant errors for elastic wave propagation (Auld 1990). In what follows we use explicit formulations for the strain tensor,

$$\varepsilon_{kl} = \frac{1}{2}\left(\frac{\partial u_l}{\partial x_k} + \frac{\partial u_k}{\partial x_l}\right),$$

where u is the displacement. The quasi-static electric field lines are perpendicular to equipotential surfaces in $E_k = -(\partial\Phi/\partial x_k)$ to develop a form of the constitutive equations suitable for the study of elastic wave propagation,

$$\sigma_{ij} = c^E_{ijkl}\varepsilon_{kl} - e_{kij}E_k = c^E_{ijkl}\frac{\partial u_l}{\partial x_k} + e_{kij}\frac{\partial \Phi}{\partial x_k}$$

$$D_j = e_{jkl}\varepsilon_{kl} + \kappa^{\varepsilon}_{jk}E_k = e_{jkl}\frac{\partial u_l}{\partial x_k} - \kappa^{\varepsilon}_{jk}\frac{\partial \Phi}{\partial x_k}.$$

If we ignore the effect of gravity on Newton's second law, an equation of motion can be written as displacement u_i as a function of time with $\partial\sigma_{ij}/\partial x_j = \rho\ (\partial^2 u_i/\partial t^2)$. From Maxwell's electrostatic equation for an insulator, the divergence is $(\partial D_j/\partial x_j) = 0 (j = 1, 2, 3)$. That is, the flux entering any element of space is exactly balanced by that leaving it. Substitution of the modified constitutive equations developed above into Newton's and Maxwell's equations yields the following differential equations:

$$\frac{\partial \sigma_{ij}}{\partial x_j} = \rho\frac{\partial^2 u_i}{\partial t^2} = c^E_{ijkl}\frac{\partial^2 u_l}{\partial x_j \partial x_k} + e_{kij}\frac{\partial^2 \Phi}{\partial x_j \partial x_k}$$

$$\frac{\partial D_j}{\partial x_j} = 0 = e_{jkl}\frac{\partial^2 u_l}{\partial x_j \partial x_k} - \kappa^{\varepsilon}_{jk}\frac{\partial^2 \Phi}{\partial x_j \partial x_k}.$$

The first equation corresponds to the equation of motion for non-piezoelectric elastic medium, with the addition of a second term on the right-hand side that adds to the elastic stiffness term. The second equation is related to the electrical displacement field, which has a divergence of zero.

We require the solution for the displacement of a monochromatic plane wave that can be described by any harmonic form as a function of time. For example, $u_k = A_k \exp i(\omega t - v_i \cdot x_i)$ where ω is the angular frequency, A_k is the amplitude, v_i is wave vector and x_i is the position vector. The solution of the system of dynamic equations for plane waves are the following equations (e.g. Royer & Dieulesaint 1996)

$$\rho V^2 p_i = \Gamma_{il}p_l + \gamma_i\Phi$$
$$0 = \gamma_l p_l - \kappa\Phi$$

with

$$\Gamma_{il} = c^E_{ijkl}n_j n_k, \quad \gamma_i = e_{kij}n_j n_k \quad \text{and} \quad \kappa = \kappa^{\varepsilon}_{jk}n_j n_k,$$

where V is the wave velocity, P_i is the particle movement or polarization direction and Γ_{il} is the familiar symmetric Christoffel tensor of a non-piezoelectric material. The three wave velocities depend on the direction of propagation (n_i). The other two terms γ_i and κ are specific quantities related to the piezoelectric properties. The scalar factor Φ of electric potential in both equations on the left-hand side may be removed by division. We therefore obtain an equation similar to the Christoffel equation for an anisotropic elastic medium plus the $\gamma_i\gamma_l/\kappa$ term (Sirotin & Shaskolskaya 1982; Royer & Dieulesaint 1996):

$$\rho V^2 p_i = \left(\Gamma_{il} + \frac{\gamma_i\gamma_l}{\kappa}\right)p_l.$$

We can now write the stiffened Christoffel tensor $\bar{\Gamma}_{il}$ of a piezoelectric material as

$$\bar{\Gamma}_{il} = \Gamma_{il} + \frac{\gamma_i\gamma_l}{\kappa}.$$

Alternatively, we write the piezoelectric stiffened elastic constants (Auld 1990; Ikeda 1990) as:

$$\bar{c}^E_{ij} = c^E_{ij} + \frac{(e_{im}n_m)(e_{mj}n_m)}{\kappa^{\varepsilon}_{kl}n_k n_l} = \boldsymbol{c}^E + \frac{(\boldsymbol{e}^{\mathrm{T}} \cdot \boldsymbol{n})(\boldsymbol{e} \cdot \boldsymbol{n})}{\boldsymbol{n}^{\mathrm{T}} \cdot \boldsymbol{\kappa}^{\varepsilon} \cdot \boldsymbol{n}}$$

and hence an alternative formulation of the stiffened Christoffel tensor is:

$$\bar{\Gamma}_{il} = \bar{c}^E_{ijkl}n_j n_k = \boldsymbol{n} \cdot \boldsymbol{c}^E \cdot \boldsymbol{n}.$$

As pointed out by Royer & Dieulesaint (1996) however, the piezoelectric stiffened elastic constants are not elastic constants in the conventional sense because of the additional piezoelectric terms, which are dependent on the propagation direction. Sirotin & Shaskolskaya (1982) and Royer & Dieulesaint (1996) suggest using the velocities calculated from $\bar{\Gamma}_{il} = \Gamma_{il} + (\gamma_i\gamma_l/\kappa)$ for practical applications. We favour the method of Ikeda (1990) and Auld (1990) as this formulation

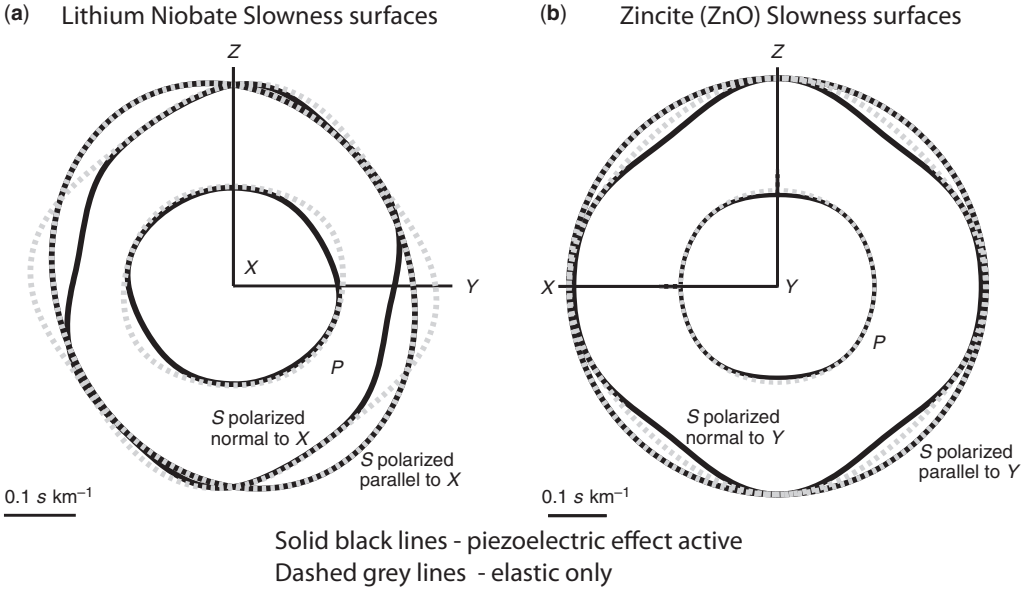

Fig. 7. Slowness surfaces for (**a**) lithium niobate (**3 m**) and (**b**) zincite (**6 mm**), where $\mathbf{X} = \mathbf{a}[2\bar{1}\bar{1}0]$, $\mathbf{Y} = \mathbf{m}[01\bar{1}0]$ and $\mathbf{Z} = \mathbf{c}[0001]$.

conserves the full tensor notation and only requires the calculation of modified stiffened elastic constants for each propagation direction, which is used in a standard Christoffel tensor calculation. From either formulation we see that the Christoffel tensor is symmetric and therefore three velocities have orthogonal polarizations as in a non-piezoelectric material. From the equation of the displacement of monochromatic plane waves and requirements of Maxwell's equations for quasi-static electrical fields it can be shown that E is parallel (longitudinal) and D, which is associated with electric power flow, is perpendicular (transverse) to the direction of propagation (n_i) in all cases (Auld 1990; Ikeda 1990). Each plane wave therefore has constant electric potential.

Applications

Elastic wave propagation

To confirm the validity of our `MTEX` code for calculating the elastic wave speed in piezoelectric crystals we have plotted the slowness (1/wave speed) surfaces of two crystals with a well-known strong coupling behaviour, lithium niobate ($LiNbO_3$) point group 3**m** (Warner *et al.*1967) and zincite (ZnO) **6mm** (Kobiakov 1980). Coupling behaviour is detected when the elastic wave speed calculated using the full piezoelectric formulation given above with stiffened elastic constants is higher than the classical elastic calculation using the ordinary stiffness constants. The plots most frequently used in crystal physics to illustrate the effect of coupling are 2D sections of the slowness surface normal to one of the tensor reference directions (X, Y or Z). Figure 7a shows the the plot for lithium niobate normal to the X direction (a-axis) in which the S waves with polarization normal to X show a strong decrease in slowness (increase in wave speed) for propagation directions near the Y-axis. In contrast, the S waves with their polarization parallel to X show no coupling effect. The P waves also exhibit a coupling effect in most propagation directions in the YZ section. Zincite is hexagonal and it elastic properties have transverse isotopic symmetry about the c-axis, so that any plane normal to the c-axis (||Z-axis) displays the same slowness surfaces. In Figure 7b we have plotted the the slowness surfaces normal to the Y direction. The P and S waves with polarization normal to Y show a reduction in slowness (increase in wave speed) typical of a coupling effect. The S wave with polarization parallel to Y shows no coupling effect. Both figures of slowness surfaces agree with previously published plots by Auld (1990) and Royer & Dieulesaint (1996). `MTEX` can plot also the wave speeds and polarizations in various pole figure plots, which allows a more complete understanding of the coupling effect.

We have also investigated the effect of piezoelectric coupling on elastic wave speeds in α-quartz.

In right- and left-handed crystals the P, S_1 and S_2 wave speeds are exactly the same along the c-axis (6.3144, 4.6884 and 4.6884 km s^{-1} respectively) with or without piezoelectric coupling. Given that the piezoelectric tensors have zero values along the c-axis (e.g. Fig. 2), this is to be expected. A potentially stronger coupling may occur along the a-axis in the basal plane where the piezoelectric tensors have their highest values. For example, the P, S_1 and S_2 wave speeds along the positive and negative a-axis are higher with coupling (0.006, 0.07 and 0.6% respectively) than an elastic calculation without coupling. These results are confirmed by the plot of the slowness in the basal plane for right- (Fig. 8a) and left-handed (Fig. 8b) quartz, in which the piezoelectric coupling has almost no effect on the the elastic wave speeds.

The effect of coupling on the elastic wave speed anisotropy is complex. For lithium niobate, which clearly has the strongest coupling, we have calculated the P-wave (AVp) and S-wave (AVs) anisotropy. With piezoelectric coupling AVp is 11.0% and AVs is 16.9%, whereas for the elastic case with no coupling AVp is 12.5% and AVs is 17.5%. For zincite with intermediate piezoelectric coupling AVp is 7.1% and AVs is 12.0%, whereas for the elastic case with no coupling AVp is 1.8% and AVs is 6.6%. Quartz, with very weak piezoelectric coupling, has AVp of 27.7% and AVs of 43.1% both with and without coupling. The effect of piezoelectric coupling on wave speed anisotropy depends on the specific 3D velocity distribution induced by the coupling. For the case of zincite, the anisotropy is multiplied by 3 for AVp and 2 for AVs.

Polycrystalline quartz vein

Previous measurements on a quartz mylonite by Bishop (1981) showed a piezoelectric effect of about 1.5% of the single crystal, whereas a quartz vein sample measured by Ghomshei *et al.* (1988) showed a maximum effect of 7% of the single crystal. Various studies from the Russian literature confirm that quartz veins frequently have a strong piezoelectric effect (Parkhomenko 1981). We therefore selected a quartzite that was probably originally a quartz vein near Tongue in the Moine Thrust zone, North Scotland. The sample has been studied previously by Lloyd *et al.* (1987) and Mainprice *et al.* (1993). A total of 382 Electron Channelling Patterns (ECPs) were recorded using a CamScan S4 scanning electron microscope (SEM) fitted with electron beam rocking coils. The patterns were indexed using both manual and computer-aided techniques. The 382 individual orientations have been indexed as right-handed crystals with the convention that the positive rhomb **r** is a stronger

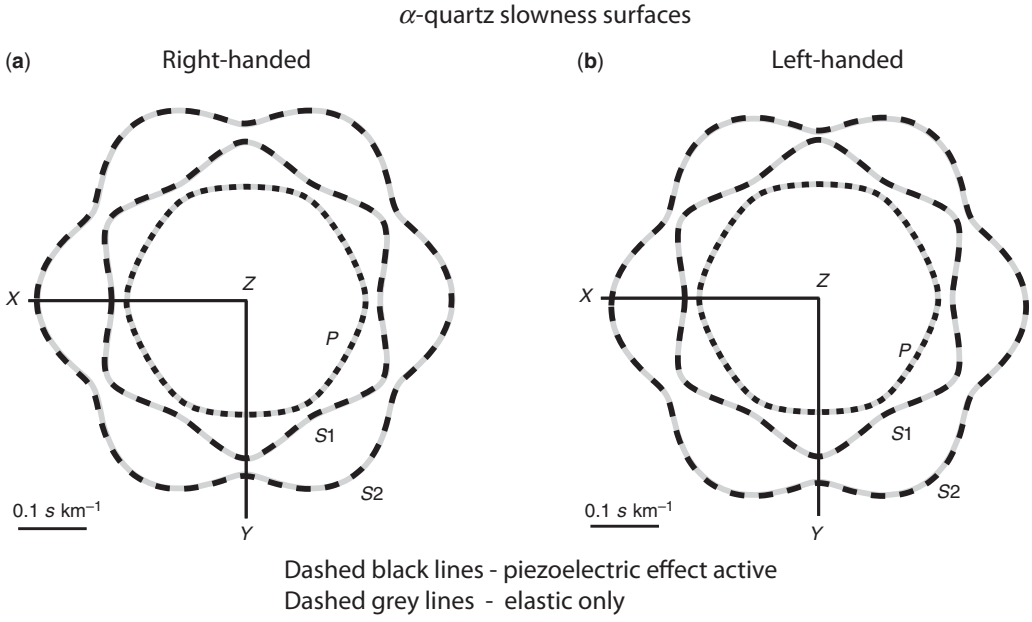

Fig. 8. Slowness surfaces for (**a**) right-handed and (**b**) left-handed α-quartz (**32**), where $\mathbf{X} = \mathbf{a}[2\bar{1}\bar{1}0]$, $\mathbf{Y} = \mathbf{m}[01\bar{1}0]$, $\mathbf{Z} = \mathbf{c}[0001]$.

reflection than the negative rhomb **z** (see Donnay & Le Page 1978). The original ECP indexing solutions have been converted to Bunge Euler angles and imported into MTEX using the EBSD generic import filter to create an object containing the individual orientation data. The orientation distribution function for right-handed indexed quartz was calculated using the default de la Vallee Poussin kernel with half-width of 10 degrees, corresponding to a harmonic expansion of 28. A list of pole figures was defined using the command Miller and the pole figures plotted with the command plotpdf.

```
% create an EBSD variable containing the data
ebsd = loadEBSD(fname, CS, SS, 'interface',
      'generic',...
  'ColumnNames', {'phi1' 'Phi' 'phi2'},
   'Bunge')
% Calculate an ODF of right - hand index quartz
odf_qtz_rh = calcODF (ebsd('Quartz'),
                      'HALFWIDTH', 10* degree)
% quartz pole figure list
% c (00.1), a (2 - 1.0), m(10.0), r (10.1),
  z (01.1) quartz
h_qtz = [Miller(0, 0, 0, 1, CS), Miller
        (2, -1, -1, 0, CS),...
Miller (1, 0, -1, 0, CS), Miller
 (1, 0, -1, 1, CS),
   Miller(0, 1, -1, 1, CS)];
% antipodal
plotpdf (odf_qtz_rh, h_qtz, 'resolution',
        5*degree, 'contourf', 'antipodal')
```

To plot inverse pole figures (IPFs) the specimen directions must be defined. In the simplest cases, the predefined Cartesian specimen coordinates xvector, yvector and zvector can be used. For specific specimen directions, the command vector3d is necessary.

```
polar_angle = 60* degree;
azimuth_angle = 45* degree;
r = vector3d ('polar', polar_angle,
              azimuth_angle);
```

For example, if we want to define two positions in pole figure coordinates labelled **A** and **P** where (i) **A** is an orientation in the $\mathbf{a}\{2\bar{1}\bar{1}0\}$ figure with high values in multiples of uniform distribution at polar angle 90° and azimuth 130° and (ii) **P** is an orientation in the $\mathbf{z}\{01\bar{1}1\}$ pole figure with a high value in multiples of uniform distribution at polar angle 90° and azimuth 220°, the inverse pole figures corresponding to specimen directions **A** and **P** can be ploted with the command plotipdf.

```
% definepole figure directions A and P
polar_angle_A = 90* degree;
azimuth_angle_A = 130* degree;
polar_angle_P = 90* degree;
azimuth_angle_P = 220* degree;
r = [vector3d('polar', polar_angle_A,
    azimuth_angle_A),...
    vector3d ('polar', polar_angle_P,
    azimuth_angle_P)];
% plot inverse pole figure
plotipdf (odf_qtz_rh, r, 'earea',
         'complete',...
   'resolution', 5* degree, 'contourf',
    'antipodal')
```

From these compact commands we can plot the pole and inverse pole figures with the 'podal' default setting or the option 'antipodal'. In MTEX 'podal' means that vectors with positive and negative ends are treated as such, and require in general to be plotted on the sphere or on two hemispheres. Other workers have referred to the 'podal' operation as 'polar' directions or vectors. The option 'antipodal' will treat a vector as an unsigned 'axis', also known as an 'non-polar' direction. All the data plotted with the 'antipodal' option can be plotted in one hemisphere.

In Figure 9 the classical pole figures used for quartz have been plotted as podal plots. The *a*-axis is the only axis that has polarity in α-quartz. In the IPF (Fig. 10) for the specimen direction 'A', the podal plot has three-fold symmetry expected for α-quartz. The highest densities in the 'A' direction IPF correspond to $+\mathbf{a}\{2\bar{1}\bar{1}0\}$ and its symmetry equivalents. The IPF for the 'P' specimen direction are almost identical between upper and lower hemispheres, with high densities parallel to the poles of $\mathbf{m}\{10\bar{1}0\}$ and $\mathbf{z}\{01\bar{1}1\}$. Note that the 'P' direction IPF also has a slightly imperfect three-fold symmetry.

The next step is to calculate the piezoelectric tensor $\boldsymbol{d}$ for our ideal right-handed α-quartz aggregate. Mainprice *et al.* (2011) describe in some detail the methods for calculating the average properties of aggregates for symmetric 2nd and 4th rank physical property tensors. Here we recall that the Voigt and Reuss averages in MTEX have been developed for individual orientations (ECP, EBSD, U-stage, etc.) as simple summations via the ODF by numerical integration or via the ODF Fourier coefficients. The route via the Fourier coefficients is particularly efficient and can be applied to ODFs of single orientations or derived from pole figure inversion. A caveat is that we have four piezoelectric tensors and their transpose for the direct and converse piezoelectric effects, respectively (see Fig. 6). However, the tensors are not symmetric and hence have no inverse. We can therefore only calculate the Voigt average tensor using the piezoelectric tensors, but not the Reuss average as this would require the inverse piezoelectric tensors which do not exist. Another caveat is that there is always some coupling in piezoelectric properties,

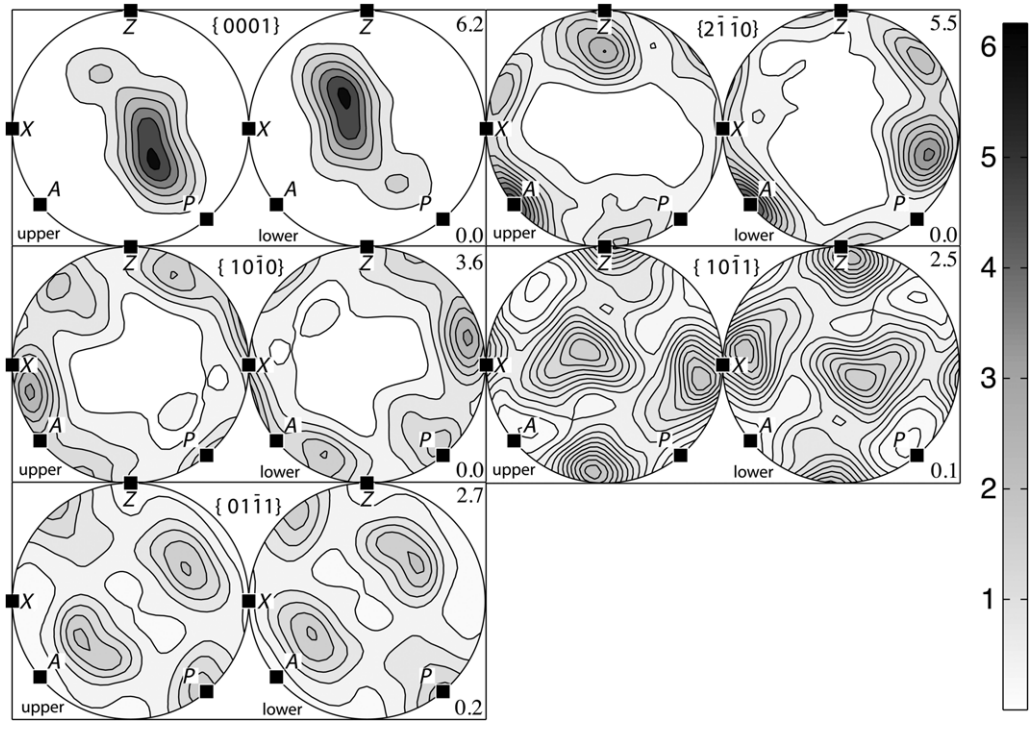

Fig. 9. Polefigure plots of **c**{0001}, **a**{2$\bar{1}\bar{1}$0}, **m**{10$\bar{1}$0}, **r**{10$\bar{1}$1}, **z**{01$\bar{1}$1} for Tongue Quartzite. The figure was generated using the 'complete' MTEX option where positive and negative crystallographic vectors are kept in their appropriate original orientations. The 'complete' plot reveals that three is a strong preference for one **a**{2$\bar{1}\bar{1}$0} pole. *X* is lineation and *Z* is the normal to the foliation. **A** marks the maximum in the **a**{2$\bar{1}\bar{1}$0} pole figure. **P** marks a high density in **a**{10$\bar{1}$0} and **z**{01$\bar{1}$1} pole figures. Left: upper hemisphere plots and right: lower hemisphere plots. Note that upper and lower hemisphere plots are rotated by 180 degrees, except for the **a**{2$\bar{1}\bar{1}$0} pole figure as positive and negative directions are not equivalent.

as described by the constitutive equations above. A simple Voigt average clearly does not explicitly take this into account. Despite these limitations, various studies have shown that the Voigt average is in reasonable agreement (within 10%) with experimental results and variational Hashin–Shtrikman upper bounds (e.g. Li and Dunn 2001; Wan *et al.* 2012).

We start with the case that we have individual orientation data g_m, $m = 1, \ldots, M$, ECP measurements and volume fractions V_m, $m = 1, \ldots, M$. The Voigt (1887, 1910) effective piezoelectric properties of aggregates are those defined by assuming that the induced tensor (in the broadest sense including vectors, e.g. the electric polarization vector for the direct effect and the elastic strain tensor for the converse effect) is everywhere homogeneous or constant (i.e. the induced tensor at every position is set equal to the macroscopic induced tensor of the specimen). The Voigt average specimen effective piezoelectric tensor $\langle d \rangle^{\mathrm{Voigt}}$ is defined by the volume average of the individual tensors $d(g_m^c)$ with crystal orientations g_m^c and volume fractions V_m,

$$\langle d \rangle^{\mathrm{Voigt}} = \sum_{m=1}^{M} V_m d(g_m^c).$$

To perform a simple summation Voigt average for piezoelectric tensor $\boldsymbol{d}$ we used the command calcTensor. We previously defined the tensor $\boldsymbol{d}$ for right-handed α-quartz. We can do the same for the left-handed α-quartz and calculate the tensors for both handedness cases.

```
% Enter Piezoelectric (strain) tensor
   (d_ij) as (3 by 6) matrix
% Md line by line in pC/N
% Ogi, H., Ohmori, T. Nakamura, N. and
   Hirao M. (2006) RH alpha - quartz
% LH alpha-quartz
   d11 = +1.9222   d14 = +0.1423
```

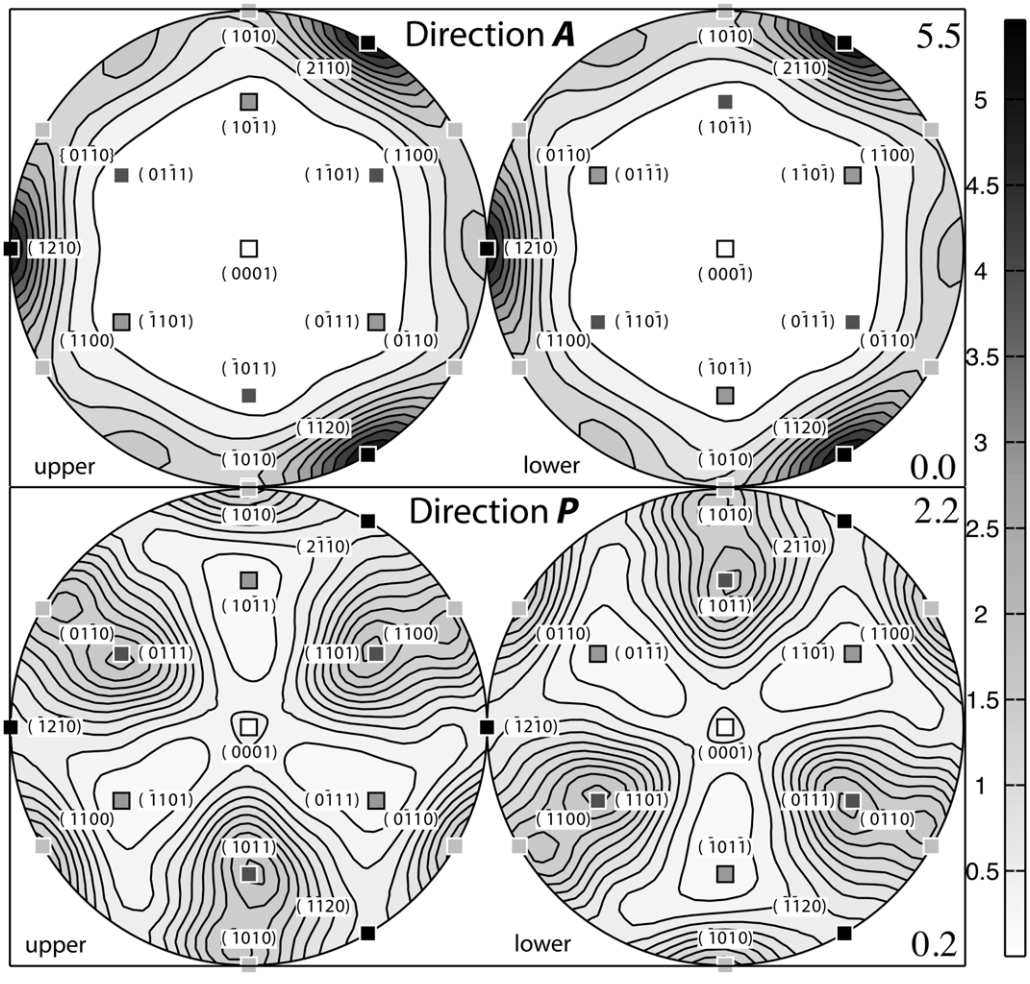

Fig. 10. The inverse pole figures (IPFs) of the specimen directions **A** (top row) and **P** (bottom row) marked on the pole figures in Figure 9. Left: upper hemisphere plots and right: lower hemisphere plots. The crystallographic directions of the pole figures are marked on the IPFs. The A-direction IPFs with the 'complete' option clearly shows a preference for + **a**{2$\bar{1}\bar{1}$0} preferred orientation with multiples of the uniform distribution reaching 5.5. The P-direction IPFs have high densities (*c.* 2.2) for **m**{10$\bar{1}$0} and **z**{01$\bar{1}$1} directions.

```
Md_LH =
[ [+1.9222 −1.9222 0 +0.1423  0        0      ];...
  [0       0       0 0       −0.1423 −3.8444];...
  [0       0       0 0        0       0      ] ];
d_LH_quartz = tensor (Md_LH, cs_Tensor,
   'rank', 3, 'propertyname',...
  'LH␣piezoelectric␣strain␣tensor',
   'unit', 'pC/N', 'DoubleConvention')
%
% Voigt average for EBSD for right - and
  left - handed alpha - quartz
%
d_RH_Voigt_Tongue_Quartzite = ...
      calcTensor (ebsd ('Quartz'),
      d_RH_quartz, 'Voigt')
```

```
d_LH_Voigt_Tongue_Quartzite = ...
     calcTensor (ebsd ('Quartz'),
     d_LH_quartz, 'Voigt')
d_RH_Voigt_Tongue_Quartzite = tensor
     (show methods, plot)
  propertyname      : RH piezoelectric
                      strain tensor
  rank              : 3 (3 × 3 × 3)
  doubleConvention : true

tensor in compact matrix form: *10^ − 2
 −8.761  23.593 −14.832 −6.251 −57.522 −23.927
 −13.01  −2.634  15.644 56.003   7.005  42.088
 −30.721 29.961   0.76  29.195 −24.565   2.078
```

```
d_LH_Voigt_Tongue_Quartzite = tensor
      (show methods, plot)
  propertyname       : LH piezoelectric
                        strain tensor
  rank               : 3 (3 × 3 × 3)
  doubleConvention : true

 tensor in compact matrix form: *10^ − 2
   8.761  −23.593   14.832    6.251   57.522   23.927
   13.01    2.634  −15.644  −56.003   −7.005  −42.088
  30.721  −29.961   −0.76   −29.195  24.565    −2.078
```

From the results (Fig. 11) it can be seen that the Voigt polycrystal average gives the same magnitudes, but the positive and negative signs are opposite between the right- and left-hand cases, just as they are in right- and left-hand single-crystal tensors ***d***. If we add right-handed single-crystal tensor ***d*** to left-handed single-crystal tensor the result is a zero-values tensor or, in other words, no piezoelectric effect. This is a situation that occurs in a single crystal if it is twinned on the Brazil law, where the host is for example right-handed and the twin will be left-handed or vice versa. Brazil twins are called 'optical' twins and Dauphiné twins are called 'electrical' twins (Frondel 1962) in the piezoelectric oscillator-plate industry, because

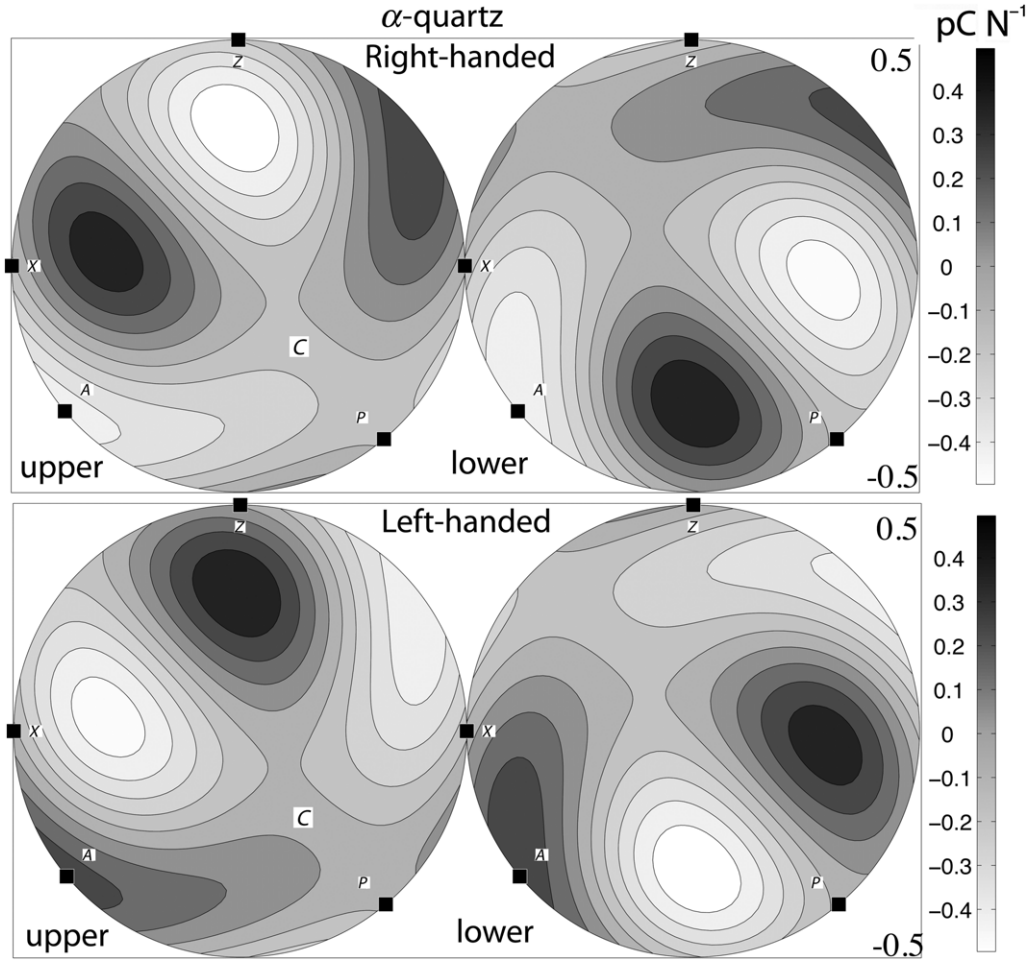

Fig. 11. The pole figures of the Voigt average for piezoelctric strain tensor ***d*** assuming all the crystals are right-handed (top) with upper (left) and lower (right) hemisphere projections. Below: assuming all the crystals are left-handed. Both right- and left-handed show extreme values near **A**, but the distribution is clearly three-dimensional as shown by the upper (left) and lower(right) hemisphere projections with approximate three-fold symmetry associated with the strong *c*-axis maximum near **C** in the upper hemisphere. *X* is lineation and *Z* is the normal to the foliation. Note that the maximum magnitude is ± 0.5 pC N^{-1}, that is, 26% of the single crystal value.

they can be detected optically and electrically, respectively. As highlighted by Donnay and Le Page (1975), both Brazil and Dauphiné twins reverse the polarity of the two-fold *a*-axes and degrade the electrical properties of the crystals, whereas only Brazil twins reverse optical activity along the *c*-axis. In the same way, if we imagined a quartz aggregate with equal volumes of right-handed and left-handed crystals, there would be no piezoelectric effect if the aggregate had topological electrical connections of all the quartz crystals. However, it should be recalled that in general the overall frequency of right- and left-handed quartz is 49.5% and 50.5%, respectively, from a total of 7335 single crystals reported by Frondel (1962) based on several studies. It is therefore classically assumed that both forms are equally likely to occur. We can plot the results for right-handed and left-handed aggregates for Voigt averages of the ***d*** tensor using the plot command (see Fig. 11).

```
% pole figure representation of d'111 the
   longitudinal
% pizezoelectric surface
plot (d_RH_Voigt_Tongue_Quartzite,
     'complete')
colorbar
% Structural reference Z-X frame and
   labels A and P
annotate (r_ZXAP, 'label',{'Z', 'X',
         'A', 'P'}, 'backgroundcolor',...
         'w', 'FontSize', 18)
% Grey scaled plots for publications
mtexColorMap white2black
```

Another important case to consider is the uniform crystallographic distribution and its effect on piezoelectric properties. Consider the case where the texture is given by an ODF f which may originate from texture modelling (Bachmann *et al.* 2010), pole figures inversion (Hielscher & Schaeben 2008), density estimation from EBSD data (Hielscher *et al.* 2010) or the present situation of a uniform ODF using the MTEX command uniformODF.

The Voigt average $\langle d \rangle^{\text{Voigt}}$ of a tensor d given an ODF f is defined by the integral

$$\langle d \rangle^{\text{Voigt}} = \int_{\text{SO(3)}} d(g) f(g) \, \mathrm{d}g.$$

Next, the ODF can be expressed as an expansion into generalized spherical harmonics of the form

$$f(g) = \sum_{\ell=0}^{r} \sum_{k,k'=-\ell}^{\ell} \hat{f}(l,\ k,\ k') D^{\ell}_{kk'}(g).$$

The Fourier method uses the expansion of the rotated tensor into generalized spherical harmonics $D^{\ell}_{kk'}(g)$. Let $d_{i_1,\ldots,i_r}$ be a piezoelectric tensor ***d*** of rank $r = 3$. Then it is well known (cf. Bunge 1969; Ganster & Geiss 1985; Mainprice & Humbert 1994; Morris 2006) that the rotated tensor $d_{i_1,\ldots,i_r}(g)$ has an expansion into generalized spherical harmonics up to order r, defined

$$d_{i_1,\ldots,i_r}(g) = \sum_{\ell=0}^{r} \sum_{k,k'=-\ell}^{\ell} \hat{d}_{i_1,\ldots,i_r}(l,\ k,\ k') D^{\ell}_{kk'}(g).$$

The explicit calculations of the coefficients $\hat{d}i_1, \ldots, i_r(l,\ k,\ k')$ are given in the appendix of Mainprice *et al.* (2011).

The average tensor with respect to this ODF can be computed using the formula

$$\frac{1}{8\pi^2}\int_{\text{SO(3)}} d_{i_1,\ldots,i_r}(g) f(g) = \frac{1}{8\pi^2}\int_{\text{SO(3)}} d_{i_1,\ldots,i_r}(g)\overline{f(g)}\,\mathrm{d}g$$

$$= \sum_{\ell=0}^{r} \frac{1}{2\ell+1} \sum_{k,k'=-\ell}^{\ell} \times \hat{d}_{i_1,\ldots,i_r}(l,k,k')\overline{\hat{f}(l,k,k')}.$$

By default, MTEX uses the Fourier approach for ODFs because it is much faster compared to the approach using a quadrature rule and is independent of any discretization. The latter approach is applied only in those cases when MTEX cannot determine the Fourier coefficients of the ODF in an efficient manner. The only case in MTEX with this problem is the Bingham orientation distribution. All the necessary calculations are done automatically, including the correction for different crystal and tensor reference frames.

To calculate the Voigt average using an ODF with the Fourier method and to obtain the most accurate results (without bias) the Dirichlet kernel with a band-width equal to the rank of the tensor property is used for piezoelectric tensors with a band-width of 3.

```
% Dirichlet kernel with Band - width = 3
K_Dirichlet = kernel ('Dirichlet',
   'bandwidth', 3)
% Calculate the uniform ODF with
   alpha - quartz
% crystal symmetry (CS) and triclinic sample
   symmetry (SS)
Uniform_Quartzite_Odf = uniformODF
   (CS, SS, 'kernel', K_Dirichlet)
% Voigt averages for RH and LH - quartz with
   uniform ODF
d_RH_Voigt_Uniform_Quartzite = ...
       calcTensor (Uniform_Quartzite_Odf,
d_RH_quartz, 'Voigt')
d_LH_Voigt_Uniform_Quartzite = ...
     calcTensor (Uniform_Quartzite_Odf,
   d_LH_quartz, 'Voigt')
```

```
d_RH_Voigt_Uniform_Quartzite = tensor
  (show methods, plot)
      rank : 3 (3 × 3 × 3)

  tensor in compact matrix form:
0 0 0 0 0 0
0 0 0 0 0 0
0 0 0 0 0 0

d_LH_Voigt_Uniform_Quartzite = tensor
(show methods, plot)
   rank: 3 (3 × 3 × 3)

  tensor in compact matrix form:
0 0 0 0 0 0
0 0 0 0 0 0
0 0 0 0 0 0
```

The results are of course the same for both right- and left-handed quartz with zero tensor ***d*** and no piezoelectric effect. For enantiomorphic crystals such as α-quartz there are two ways of obtaining no piezoelectric effect: equal volumes of right- and left-handed crystals with the same ODF or a uniform distribution of crystal orientations. In addition, for the case of α-quartz, both Brazil and Dauphiné twins reduce the piezoelectric effect. For all aggregates of piezoelectric crystals, a uniform distribution of crystal orientations will result in no piezoelectric effect. Clearly the strategy for piezoelectric polycrystalline ferroelectric ceramics (e.g. lead zirconate titanate $PbZr_{1-x}$ Ti_xO_3, Newnham 2005) is to optimize the ODF to obtain the desired piezoelectric effect by various electrical and mechanical processes, which is referred to as poling. In geological samples such as quartzites the maximum piezoelectric effect will occur if all crystals are of one handedness (e.g. right-handed) and the ODF is as close as possible to a single crystal. That is, the point maxima for the *c*-axis and + *a*-axis pole figures have developed three-fold symmetry. Quartzites with such CPO occur in the amphibolite facies Saxony granulites (e.g. Schmid *et al.* 1981; Schmid & Casey 1986).

Until now, the geological view of the probability of finding right- or left-handed quartz crystals was based on the studies reported by Frondel (1962), where the frequency is nearly 50%:50%. These studies were based on measurements of large single crystals rather than polycrystalline aggregates. In chemistry, it has been shown that two types of crystalline solids can be formed by chiral (enantiomorphic) crystals: 'racemic' aggregates of 50%:50% right- and left-handed crystals; and 'homochirality' aggregates composed uniquely of right- or left-handed forms. The latter originate by some 'symmetry breaking' process that creates an imbalance between left and right enantiomorphic crystals. The degree of imbalance is measured by crystal enantiomorphic excess or $CEE = (N_R - N_L)/(N_R + N_L)$, where N_R and N_L are the number of right- and left-handed crystals. Over 100 years ago, Kipping & Pope (1898) showed that seeding a crystallizing solution of sodium chlorate ($NaClO_3$ cubic space group $\mathbf{P2_13}$, point group **23**) with right- or left-handed crystal would result in an aggregate of uniquely one-hand. A number of experiments conducted in recent years on sodium chlorate have shown that the simple action of stirring crystals floating in solution will cause homochirality (e.g. Kondepudi *et al.* 1990; Viedma 2004; Veintemillas-Verdaguer *et al.* 2007). Similarly, stirred crystallization of melt (Kondepudi *et al.* 1999), crushing or grinding of crystals (Viedma 2005), boiling solutions with temperature gradient (El Hachemi *et al.* 2009; Viedma & Cintas 2011) or shaking solutions of millimetre-sized crystals (Viedma *et al.* 2013) can also cause homochirality. All of these processes are likely to occur in tectonic or volcanic environments within the Earth. Although the mechanism responsible for homochirality of the crystal aggregates remains controversial, experimental results have been reproduced by several laboratories (see reviews by Weissbuch & Lahav 2011; Cintas & Viedma 2012). While no similar experiments have been conducted on quartz, it would be surprising if similar effects did not occur for natural crystals to explain the probable increased homochirality in vein quartz.

Idealized symmetry models of piezoelectric properties of quartz aggregates have been proposed by Zheludev (1974) and used by Parkhomenko (1971) and Bishop (1981). We develop here the modelling of polycrystalline aggregates of Zheludev (1974) by using the ideal symmetry groups with *n*-fold axis, where $n = \infty$ are called limiting or Curie groups. There are seven limiting groups, but only three (**∞**,**∞mm** and **∞2**) do not have a centre of symmetry and hence can have piezoelectric properties (e.g. Zheludev 1974). Both ∞ and **∞mm** and have a unique polar axis and could potentially be associated with CPO of α-quartz. For example, an ideal ∞ right-handed quartz CPO would have the ∞-fold axis parallel to the quartz a1 $[2\bar{1}\bar{1}0]$. This can be implemented by MTEX as:

```
% Default Dirichlet kernel when calculating
   physical properties from odf
% Band − width = Lmax=3 for piezoelectric
   properties (tens or 3th rank)
% axial direction : a1 = [2 − 1 − 10] quartz
  a1_direction = Miller (2, −1, −1, 0, CS,
    'uvw', 'phase', 'Quartz')
% setup Dirichlet kernel
K_Dirichlet = kernel ('Dirichlet',
                'bandwidth', 3)
```

```
% calcluate fibre odf with a1 crystal
   parallel x specimen
Odf_Model_A_Dirichlet = fibreODF
   a1_direction, zvector, K_Dirichlet)
% RH Voigt average from odf_qtz_fourier
[d_RH_Voigt_Model_A_Quartzite_ODF_
   Dirichlet] = ...
    calcTensor (Odf_Model_A_Dirichlet ,...
    d_RH_quartz, 'Voigt')

a1_direction = Miller (show methods, plot)
  size : 1 x 1
  options: uvw
  mineral : Quartz (-3m, X|| a*, Y|| b, Z|| c*)
  u 2
  v -1
  t -1
  w  0

K_Dirichlet = kernel (show methods, plot)
  type: Dirichlet, hw = 37

Odf_Model_A_Dirichlet = ODF(show methods,
   plot)
  crystal symmetry: Quartz(-3m, X|| a* ,
   Y|| b, Z|| c*)
  sample symmetry : triclinic

  Fibre symmetric portion:
    kernel: Dirichlet, hw = 37
    center: <2 -1 -10> -001
    weight: 1

d_RH_Voigt_Model_A_Quartzite_ODF_
   Dirichlet =tensor (show methods, plot)
  rank: 3 (3 x 3 x 3)

tensor in compact matrix form:
     0      0         0  0.0356    0.9611   0
     0      0         0  0.9611   -0.0356   0
0.9611 0.9611   -1.9222       0         0   0
```

From this calculation we deduce that the **∞** $d_{31} = d_{32} = d_{24} = d_{15}$ = single-crystal quartz $-d_{11}/2$, d_{33} = single-crystal quartz d_{11} and d_{14} and d_{25} = single-crystal quartz $-d_{14}/4$ and $d_{14}/4$, respectively. Figure 12 shows the maximum value of -1.92 pC N^{-1} parallel to X, as expected. The value is 100% of the single crystal in the +a1[$2\bar{1}\bar{1}0$] direction, confirming that no bias or smoothing is introduced into the ODF when using the Dirichlet kernel for physical properties. The **∞mm** symmetry would require more complex microstructure in an aggregate composed of right- and left-handed crystals with ∞-fold axis parallel to the quartz a1[$2\bar{1}\bar{1}0$] direction as before, but now with two mirror planes (one normal to the symmetry axis and parallel to the symmetry axis) resulting in four-fold disposition of the positive $a1$-axis in the basal plane (Zheludev 1974); this seems unlikely in quartz. Alternatively, it is more probable in tourmaline **3m** point group symmetry with mirror planes. The **∞2** symmetry

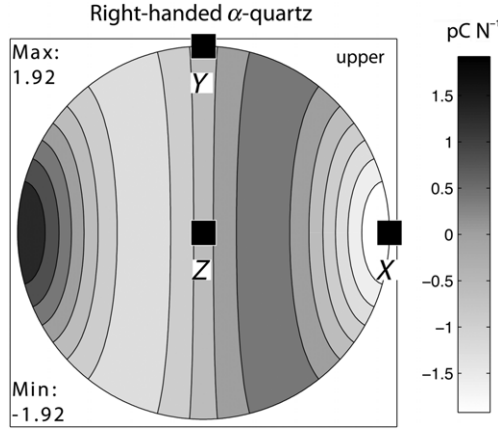

Fig. 12. Pole figure of the Voigt average for the piezoelectric strain tensor ***d*** for right-handed α-quartz assuming the **∞** Curie group symmetry with the positive a_1-axis parallel to the ∞-fold symmetry axis. The Voigt average was calculated using an ODF constructed using fibreODF command with Dirichlet kernel and band-width of three. Upper hemisphere projection. *X* is lineation and *Z* is the normal to the foliation. Note that the maximum magnitude is ± 1.92 pC N^{-1}, that is, 100% of the single crystal value.

with a two-fold axis normal to the symmetry axis has no polar axes. This symmetry of the piezoelectric property could result from right-handed quartz with a CPO having the ∞-fold axis parallel to both the quartz c[0001] and the specimen z-direction and two-fold a-axes normal to the symmetry axis. By performing a similar calculation to above, we find that the only two non-zero coefficients are d_{14} and d_{25}, equal to the single-crystal quartz $d_{14}/2$ and $-d_{14}/2$, respectively. There are no polar axes because the only non-zero coefficients are two shear terms (d_{14} and d_{25}) and no polarization can be generated parallel to compressive stress (longitudinal effect), and piezoelectric polarization can only be generated by applying shear stresses. The **∞2** has the same non-zero coefficients as the crystal point groups **422** and **622**, for which we demonstrated that $d'_{11} = 0 = 0$.

Conclusions

We have extended the functions of MTEX to include the calculation of anisotropic crystal physical properties of 3rd rank Cartesian tensors. The functions can be applied to tensors of single or polycrystalline materials. The implementation of the average tensor of polycrystalline and multi-phase aggregates using the Voigt average has been made using three

methods: (a) the weighted summation for individual orientation data (e.g. EBSD, ECPs); (b) the weighted integral of the ODF; and (c) the Fourier coefficients of the ODF. Special attention has been paid to the crystallographic reference frame used for orientation data (e.g. Euler angles) and Cartesian tensors, as they dependent on the origin of the orientation and tensor data. Specifically, piezoelectric properties in the 2D and 3D representations allow a better appreciation of the often-complex 3D distribution of the different electrical polarizations and their signs. Uniform ODFs will result in a zero piezoelectric tensor for all aggregates of piezoelectric crystals. Enantiomorphic crystal aggregates composed of equal volumes of right- and left-handed crystals with the same ODF will also result in a zero piezoelectric tensor. Processes such as stirring or shaking crystals floating in solution and crushing or grinding can cause homochirality, leading to aggregates with a high piezoelectric anisotropy. When searching for ODFs that will produce aggregates with a maximum piezoelectric effect, a good understanding of the single-crystal properties is essential. In the case of quartz, the so-called *Y* maximum CPO with *c*-axis parallel to the specimen *Y*-axis would appear to be a good candidate. While the elastic wave velocity is virtually unaffected (less than 1%) by piezoelectric coupling for quartz, in other materials the effect is very important as the wave speed anisotropy may be increased by a factor of 2–3 (e.g. zincite). In other examples there is almost no effect. The effect of the ODF can be investigated by using the `fibreODF` command, either a simple verification of the Curie symmetry group for α-quartz as illustrated here or using a combination of model ODFs.

The ensemble of MTEX functions can be used to construct project-specific MatLab M-files to process orientation data of any type in a coherent workflow from the texture analysis to the anisotropic physical properties. A wide range of graphical tools provides publication-quality output in a number of formats. The construction of M-files for specific problems provides a problem-solving method for teaching elementary to advanced texture analysis and anisotropic physical properties. The open-source nature of this project (http://mtex.googlecode.com) allows researchers to access all the details of their calculations, check intermediate results and further the project by adding new functions on Linux, Mac OS X or Windows platforms.

It is pleasure for DM to dedicate this paper to Professor Ernie Rutter who introduced him to the representation of physical properties of crystals by tensors as part of his Masters course at Imperial College, London. This contribution is the result of scientific cooperation on the research project 'Texture and Physical Properties of Rocks', funded by the French–German program EGIDE-PROCOPE. This bilateral program is sponsored by the German Academic Exchange Service (DAAD) with financial funds from the Federal Ministry of Education and Research (BMBF) and the French Ministry of Foreign Affairs. The authors thank the two reviewers for the hard work involved in reviewing such a technical manuscript; their checking of some of the equations eliminated some typing errors and helpful comments greatly improved our paper.

References

ANSI-IEEE 176 1987. Standard on Piezoelectricity, http://dx.doi.org/10.1109/IEEESTD.1988.79638

Auld, B. A. 1990. *Acoustic Fields and Waves in Solids (Two Volumes)*. Krieger Publishing Co., Malabar, Florida.

Bachmann, F., Hielscher, H., Jupp, P. E., Pantleon, W., Schaeben, H. & Wegert, E. 2010. Inferential statistics of electron backscatter diffraction data from within individual crystalline grains. *Journal of Applied Crystallography*, **43**, 1338–1355.

Bazhenov, A. V. 1961. *Piezoelectric Properties of Wood*. Consultants Bureau, New York.

Bechmann, R. 1958. Elastic and piezoelectric constants of alpha-quartz. *Physical Review*, **110**, 1060–1061.

Bishop, J. R. 1981. Estimating quartz fabrics from piezoelectric measurements. *Mathematical Geosciences*, **13**, 261–289.

Bishop, J. R. & Emerson, D. W. 1999. Geophysical properties of zinc-bearing deposits. *Australian Journal of Earth Sciences*, **46**, 311–328.

Bond, W. L. 1943. The mathematics of the physical properties of crystals. *Bell System Technical Journal*, **XXII**, 1–72.

Brainerd, J. G. *et al.* 1949. Standards on piezoelectric crystals. *Proceedings of the Institute of Radio Engineers*, **37**, 1378–1395.

Bunge, H. J. 1969. *Mathematische Methoden der Texturanalyse*. Akademie-Verlag, Berlin.

Bunge, H. J. & Esling, C. 1985. Symmetries in texture analysis. *Acta Crystallographica*, **A41**, 59–67.

Cady, W. G. 1964. *Piezoelectricity*. Dover Publications Inc., New York.

Cintas, P. & Viedma, C. 2012. On the physical basis of asymmetry and homochirality. *Chirality*, **24**, 894–908.

Cook, R. K. & Weissler, P. G. 1950. Piezoelectric constants of alpha- and beta-quartz at various temperatures. *Physical Review*, **80**, 712–716.

Corry, C. E. 1994. Investigation of ferroelectric effects in two sulfide deposits. *Journal of Applied Geophysics*, **32**, 55–72.

Curie, J. & Curie, P. 1880. Développement par compression de l' électricité polaire dans les cristaux hémièdres à faces inclinées. *Bulletin de la Société Minéralogique de France*, **3**, 90–93.

Curie, J. & Curie, P. 1881. Contractions et dilatations produites par des tensions électriques dans les cristaux hémièdres à faces inclinées. *Comptes Rendus (France)*, **93**, 1137–1140.

Curie, J. & Curie, P. 1882. Phénomènes électriques des cristaux hémièdres à faces inclinées. *Journal de Physique Théorique et Appliquée*, **1**, 245–251.

DONNAY, J. D. H. & LE PAGE, Y. 1975. Twin laws v. electrical and optical characters in low quartz. *Canadian Mineralogist*, **13**, 83–85.

DONNAY, J. D. H. & LE PAGE, Y. 1978. The vicissitudes of the low quartz setting or the pitfalls of enantiomorphism. *Acta Crystallographica*, **A34**, 584–594.

EL-HACHEMI, Z., CRUSATS, J., RIBO, J. M. & VEINTEMILLAS-VERDAGUER, S. 2009. Spontaneous transition toward chirality in the $NaClO_3$ crystallization in boiling solutions. *Crystal Growth & Design*, **9**, 4802–4806.

FRONDEL, C. 1962. *The System of Mineralogy*, 7th edn. Silica Minerals. John Wiley, New York.

FUKADA, E. & YASUDA, I. 1957. On the piezoelectric effect of bone. *Journal of the Physical Society of Japan*, **12**, 1158–1162.

FUKADA, E. & YASUDA, I. 1964. Piezoelectric effects in collagen. *Japanese Journal of Applied Physics*, **3**, 117–121.

GANSTER, J. & GEISS, D. 1985. Polycrystalline simple average of mechanical properties in the general (triclinic) case. *Physica Status Solidi (b)*, **132**, 395–407.

GHOMSHEI, M. M., NAROD, B. B., TEMPLETON, T. L., ARROTT, A. S. & RUSSELL, R. D. 1988. Piezoelectric pole figure of a vein quartz sample. *Textures Microstructures*, **7**, 303–316.

GOODMAN, P. & JOHNSTON, A. W. S. 1977. Identification of enantiomorphously related space groups by electron diffraction – a second method. *Acta Crystallographica*, **A33**, 997–1001.

GOODMAN, P. & SECOMB, T. W. 1977. Identification of enantiomorphously related space groups by electron diffraction. *Acta Crystallographica*, **A33**, 126–133.

HAUSSÜHL, S. 1991. Pyroelectric, dielectric, piezoelectric, elastic and thermoelastic properties of triclinic lithium hydrogen Oxalate monohydrate, $LiHC_20_4.H_20$. *Zeitschrift für Kristallographie*, **194**, 57–65.

HAYAKAWA, R. & WADA, Y. 1973. Piezoelectricity and related properties of polymer films. *Advances in Polymer Science*, **11**, 1–55.

HECKMANN, G. 1925. Die Gittertheorie der festen Köper. *Ergeb Exakten Naturwiss*, **4**, 100–153.

HERMANN, C. 1934. Tensoren und Kristallsymmetrie. *Zeitschrift für Kristallographie*., **89**, 32–48.

HIELSCHER, R. & SCHAEBEN, H. 2008. A novel pole figure inversion method: specification of the MTEX algorithm. *Journal of Applied Crystallography*, **41**, 1024–1037, http://dx.doi.org/10.1107/S002188980 8030112

HIELSCHER, R., SCHAEBEN, H. & SIEMES, H. 2010. Orientation distribution within a single hematite crystal. *Mathematical Geosciences*, **42**, 359–375.

IKEDA, T. 1990. *Fundamentals of Piezoelectricity*. Oxford University Press.

JAFFE, B., COOK, W. R. & JAFFE, H. 1971. *Piezoelectric Ceramics*. Academic Press, New York.

JUNG, I. H. & AUH, K. H. 1999. Crystal growth and piezoelectric properties of langasite ($La^3Ga^5SiO^{14}$) crystals. *Materials Letters*, **41**, 241–246.

KERKOC, P., MARUO, S., HORINOUCHI, S. & SASAKI, K. 1999. Piezoelectric and electro-optic coefficients of the molecular nonlinear optical crystal 2-furyl methacrylic anhydride. *Applied Physics Letters*, **74**, 3105–3106.

KIPPING, W. S. & POPE, W. J. 1898. Enantiomorphism. *Journal of the Chemical Society, Transactions*, **73**, 606–617.

KLAPPER, H. & HAHN, Th. 2006. Point-group symmetry and physical properties of crystals. *In*: *International Tables for Crystallography*. Kluwer Academic Publishers, Dordrecht.

KOBIAKOV, I. B. 1980. Elastic, Piezoelectric and dielectric properties of ZnO and CdS single crystals in a wide range of temperatures. *Solid State Communications*, **35**, 305–310.

KONDEPUDI, D. K., KAUFMANN, R. & SINGH, N. 1990. Chiral symmetry breaking in sodium chlorate crystallization. *Science*, **250**, 975–976.

KONDEPUDI, D. K., LAUDADIO, J. & ASAKURA, K. 1999. Chiral symmetry breaking in stirred crystallization of 1, 1′-binaphthyl melt. *Journal of the American Chemical Society*, **121**, 1448–1451.

LE PAGE, Y., SAXE, P. & RODGERS, J. R. 2002. *Ab initio stiffness for low quartz and calcite*. *Physica Status Solidi (b)*, **229**, 1155–1161.

LI, J. Y. & DUNN, M. L. 2001.Variational bounds for the effective moduli of heterogeneous piezoelectric solids. *Philosophical Magazine A*, **81**, 903–926.

LIPPMANN, G. 1881. Principe de la conservation de l'électricité. *Annales de Chimie et de Physique*, **24**, 145–177.

LLOYD, G. E., FERGUSON, C. C. & LAW, R. D. 1987. Discriminatory petrofabric analysis of quartz rocks using SEM electron channelling. *Tectonophysics*, **135**, 243–249.

MAINPRICE, D. & HUMBERT, M. 1994. Methods of calculating petrophysical properties from lattice preferred orientation data. *Surveys in Geophysics*, **15**, 575–592.

MAINPRICE, D., LLOYD, G. E. & CASEY, M. 1993. Individual orientation measurements in quartz polycrystals-advantages and limitations for texture and petrophysical property determinations. *Journal of Structural Geology*, **15**, 1169–1187.

MAINPRICE, D., HIELSCHER, R. & SCHAEBEN, H. 2011. Calculating anisotropic physical properties from texture data using the MTEX open-source package. *In*: PRIOR, D. J., RUTTER, E. H. & TATHAM, D. J. (eds) *Deformation Mechanisms, Rheology and Tectonics: Microstructures, Mechanics and Anisotropy*. Geological Society, London, Special Publications, **360**, 175–192, http://dx.doi.org/10.1144/SP360.10

MARTHINSEN, K. & HØIER, R. 1988. On the breakdown of Friedel's law in electron backscattering. *Acta Crystallographica*, **A44**, 700–707.

MASON, W. P. 1966. *Crystal Physics of Interaction Processes*. Academic Press, New York.

MESSING, G. L., TROLIER-MCKINSTRY, S. *ET AL.* 2004. Templated Grain Growth of Textured Piezoelectric Ceramics. *Critical Reviews in Solid State and Materials Sciences*, **29**, 45–96.

MORRIS, P. R. 2006. Polycrystalline elastic constants for triclinic crystal and physical symmetry. *Journal of Applied Crystallography*, **39**, 502–508.

NEISHTADT, N. M., EPPELBAUM, L. V. & LEVITSKI, A. G. 2006. Application of piezoelectric and seismoelectrokinetic phenomena in exploration geophysics: Review of Russian and Israeli experiences. *Geophysics*, **71**, B41–B53, http://dx.doi.org/10.1190/1.2187714

NEWNHAM, R. E. 2005. *Properties of Materials Anisotropy, Symmetry, Structure*. Oxford University Press, Oxford.

NYE, J. F. 1985. *Physical Properties of Crystals: Their Representation by Tensors and Matrices*, 2nd edn. Oxford University Press, England.

OGI, H., FUKUNAGA, M. & MASAHIKO HIRAO, M. 2004. Elastic constants, internal friction, and piezoelectric coefficient of α–TeO_2. *Physical Review B*, **69**, 024104.

OGI, H., OHMORI, T., NAKAMURA, N. & HIRAO, M. 2006. Elastic, anelastic and piezoelectric coefficients of alpha-quartz determined by resonance ultrasound spectroscopy. *Journal of Applied Physics*, **100**, 053511.

PANDEY, C. S. & SCHREUER, J. 2012. Elastic and piezoelectric constants of tourmaline single crystals at nonambient temperatures determined by resonant ultrasound spectroscopy. *Journal of Applied Physics*, **111**, 013516, http://dx.doi.org/10.1063/1.3673820

PARKHOMENKO, E. I. 1971. *Electrification Phenomenia in Rocks*. Plenum Press, New York.

REUSS, A. 1929. Berechnung der Fließrenze von Mischkristallen auf Grund der Plastizitätsbedingung für Einkristalle. *Zeitschrift für Angewandte Mathematik und Mechanik*, **9**, 49–58.

ROYER, D. & DIEULESAINT, E. 1996. *Ondes élastiques dans les solides*. Tome 1, Propagation libre et guidée, Masson, Paris.

RUSSELL, R. D. & GHOMSHEI, M. M. 1997. Inverting piezoelectric measurements. *Tectonophysics*, **271**, 21–35.

SCHMID, S. M. & CASEY, M. 1986. Complete fabric analysis of some commonly observed quartz c-axis patterns. *In*: HEARD, H. C. & HOBBS, B. E. (eds) *Mineral and Rock Deformation: Laboratory Studies, The Paterson Volume, Series*. AGU monograph, Washington, **36**, 263–286.

SCHMID, S. M., CASEY, M. & STARKEY, J. 1981. An illustration of the advantage of a complete texture analysis described by the orientation distribution function (ODF) using quartz pole figure data. *Tectonophysics*, **78**, 101–117.

SIROTIN, Yu. I. & SHASKOLSKAYA, M. P. 1982. *Fundamentals of Crystal Physics*. Mir, Moscow.

TAYLOR, S. R. & MCLENNAN, S. M. 1985. *The Continental Crust: Its Composition and Evolution*. Blackwell, Oxford.

TICHÝ, J., ERHART, J., KITTINGER, E. & PŘÍVRATSKÁ, J. 2010. *Fundamentals of Piezoelectric Sensorics*. Springer-Verlag, Berlin.

VEINTEMILLAS-VERDAGUER, S., OSUNA ESTEBAN, S. & HERRERO, M. A. 2007. The effect of stirring on sodium chlorate crystallization under symmetry breaking conditions. *Journal of Crystal Growth*, **303**, 562–567.

VIEDMA, C. 2004. Experimental evidence of chiral symmetry breaking in crystallization from primary nucleation. *Journal of Crystal Growth*, **261**, 118–121.

VIEDMA, C. 2005. Chiral symmetry breaking during crystallization: Complete chiral purity induced by nonlinear autocatalysis and recycling. *Physical Review Letters*, **94**, 065504.

VIEDMA, C. & CINTAS, P. 2011. Homochirality beyond grinding: deracemizing chiral crystals by temperature gradient under boiling. *Chemical Communications*, **47**, 12786–12788.

VIEDMA, C., MCBRIDE, J. M., KAHR, B. & PEDRO CINTAS, P. 2013. Enantiomer-specific oriented attachment: formation of macroscopic homochiral crystal aggregates from a Racemic System. *Angewandte Chemie International Edition*, **52**, 10545–10548.

VOIGT, W. 1887. Theoretische studien über die elastizitätsverhältnisse. *Abhandlungen der Akademie der Wissenschaften in Göttingen*, **34**, 48–55.

VOIGT, W. 1898. *Die Fundamentalen Physiklischen Eigenschaften der Kristalle*. Teubner-Verlag, Leipzig.

VOIGT, W. 1910. *Lehrbuch der Kristallphysik*. Teubner-Verlag, Leipzig.

VOIGT, W. 1928. *Lehrbuch der Kristallphysik*. Teubner-Verlag, Leipzig.

WAN, Y. P., XIE, L. T. & ZHONG, Z. 2012. Variational bounds of the effective moduli of piezoelectric composites. *Science China Physics, Mechanics and Astronomy*, **55**, 2106–2113, http://dx.doi.org/10.1007/s11433-012-4706-9

WARNER, A. W., ONOE, M. & COQUIN, G. A. 1967. Determination of Elastic and Piezoelectric Constants for Crystals in Class (3 m). *Journal of the Acoustical Society of America*, **42**, 1223–1231.

WEISSBUCH, I. & LAHAV, M. 2011. Crystalline architectures as templates of relevance to the origins of homochirality. *Chemical Reviews,* **111**, 3236–3267, http://dx.doi.org/10.1021/cr1002479

WENK, H.-R. 1985. Measurement of pole figures. *In*: WENK, H.-R. (ed.) *Preferred Orientation in Metals and Rocks: An Introduction to Modern Textural Analysis*. Academic Press, Orlando.

ZHELUDEV, I. S. 1974. Piezoelectricity in textured media. *Solid State Physics*, **29**, 315–360.